

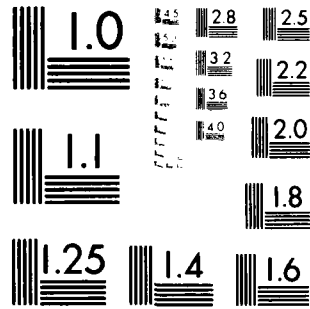
AD-A116 162

WASHINGTON UNIV SEATTLE DEPT OF ELECTRICAL ENGINEERING F/6 20/12
CONTROL OF GAAS MICROWAVE SCHOTTKY DIODE ELECTRICAL CHARACTERIS--ETC(U)
MAY 82 S J TENG, R E GOLDWASSER N00014-79-C-0840
TR-ONR-82-1 NL

UNCLASSIFIED

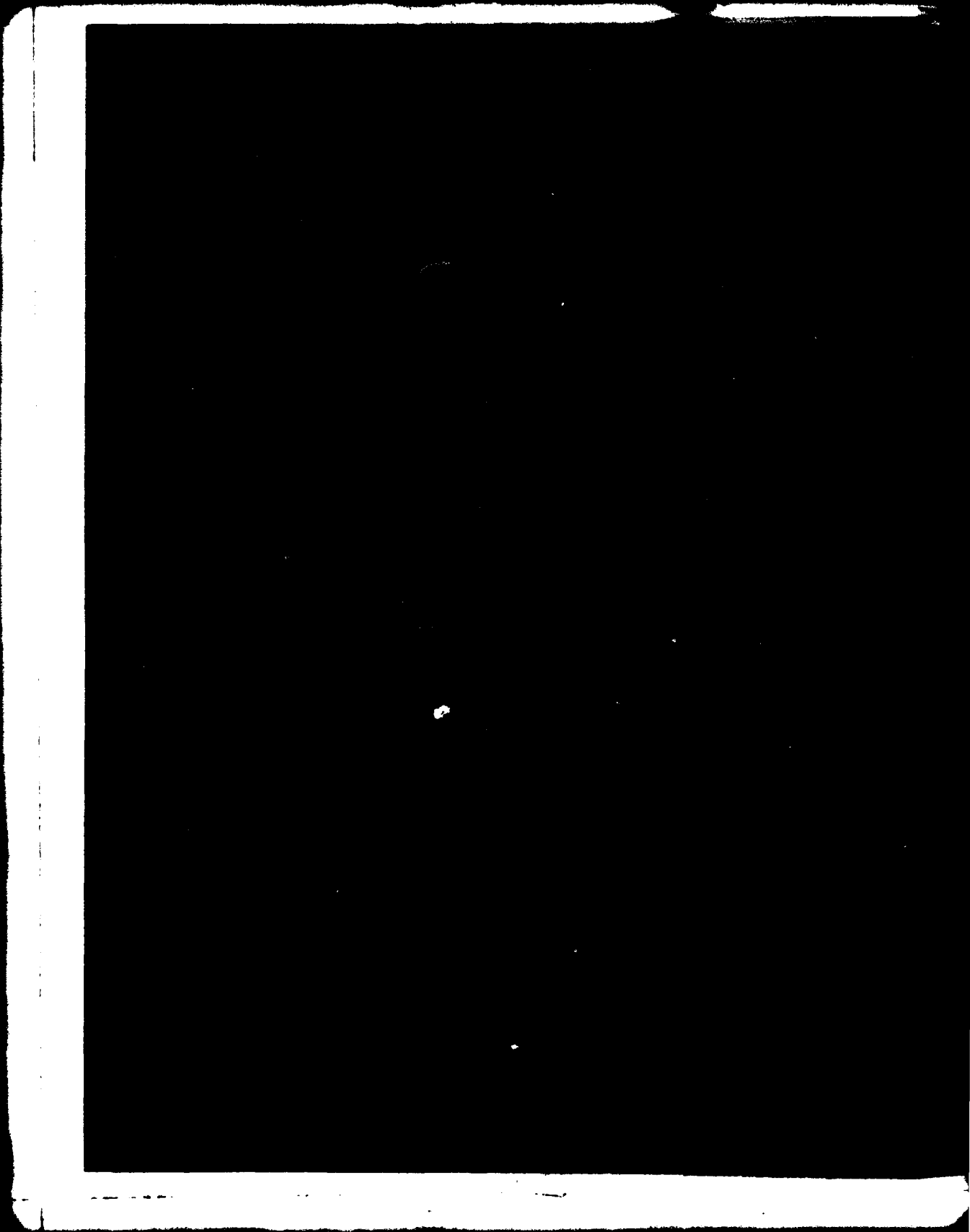
1 of 2





MICROCOPY RESOLUTION TEST CHART
NATIONAL BUREAU OF STANDARDS 1963-A

AD A116162





WASHINGTON
UNIVERSITY
IN ST. LOUIS

12

CONTROL OF GaAs MICROWAVE SCHOTTKY DIODE ELECTRICAL CHARACTERISTICS BY CONTACT GEOMETRY: THE GAP DIODE

S.J.J. TENG
R.E. GOLDWASSER
F.J. ROSENBAUM

Department of Electrical Engineering
Washington University
St. Louis, Mo. 63130

MAY 1982

DTIC
ELECTE
JUN 29 1982
S H D

TECHNICAL REPORT ONR-82-1

Office of Naval Research
Arlington, VA 22217

Reproduction, in whole or in part, is permitted for any purpose of the U.S. Government.

Contract: N00014-79-C-840
Contract Authority: NR SRO-004

Approved for public release; distribution unlimited.

TABLE OF CONTENTS

No.		Page
1.	Introduction	1
1.1	Metal-Semiconductor Schottky-Barrier	2
1.2	Metal-Semiconductor Barrier Height	3
1.3	Control of Barrier Height	6
1.3.1	Highly Electronegative Contacts	6
1.3.2	Doping Variations Near the Contact	7
1.3.2.1	Alloying	7
1.3.2.2	Ion Implantation	8
1.3.2.3	Ion Bombardment	8
1.3.3	Thin Interfacial Insulating Layers	8
1.3.4	Edge Tunneling	9
1.3.5	Gap-Controlled Low Barrier	9
2.	Gap-Controlled (Low Barrier) Schottky Diode	11
2.1	Schottky-Barrier Model	11
2.2	Ohmic Contact to GaAs	16
2.3	Theory of Gap-Controlled Charge Transport	18
2.3.1	Basic Characteristics	18
2.3.2	Current-Voltage Relationship	24
2.3.2.1	Notched-type Gap Diode	24
2.3.2.2	Planar-type Gap Diode	29
3.	Vapor-Phase Epitaxial Growth of GaAs	37
3.1	Description of Epitaxial Reactor	37
3.2	Source Saturation	40
3.3	Epitaxial Growth Procedure	42
3.4	H ₂ S Dopant Incorporation	44
3.5	Substrate Preparation	45
3.6	Material Evaluation	45



Accession For
 DTIC GRA&I
 DTIC TAB
 Unannounced
 Justification

By _____

Distribution/Availability Codes
 Avail and/or Special

Dist _____

A

TABLE OF CONTENTS
(continued)

No.	Page
4. Device Fabrication	49
4.1 Device Construction	49
4.2 Ohmic Contact Fabrication	49
4.3 Schottky-Barrier Fabrication	52
4.4 Junction Formation	55
4.5 GaAs Mesa Etch and SiO Insulation	57
4.6 Diode Packaging	57
5. Experiment Results and Discussion	62
5.1 Current-Voltage Characteristics	62
5.2 Diode Capacitance	70
5.3 Temperature Dependence of the I-V Characteristics	72
5.4 Detector Characteristics	77
5.5 Mixer Characteristics	80
6. Conclusions	85
7. Acknowledgement	88
8. Bibliography	89

LIST OF FIGURES

No.		Page
1.	Schematic representation of electric field and potential resulting from surface states in the Schottky-barrier depletion region	4
2.	Experimental barrier heights for metal contacts to n-type Si, GaAs, GaP and CdS [4]	5
3.	One-dimensional parabolic depletion layer potential energy barrier for an n-type semiconductor. Image force rounding of the barrier shape is neglected	12
4.	Schematic diagram of gap-controlled Schottky diode (a) notched type (b) planar-type	19
5.	Cross-sectional view of notched-type gap-controlled Schottky diode with applied bias voltage V_A	22
6.	Calculated forward I-V characteristics of the notched-type Gap diode from Equation (2.19) as a function of ohmic gap width W	27
7.	Calculated relationship between the turn-on voltage (at $I_A = 1$ mA), ohmic gap width W and semiconductor carrier concentration N_D of the notched-type Gap diode	28
8.	Calculated relationship between the turn-on voltage (at $I_A = 1$ mA), ohmic gap width W and semiconductor channel length ℓ of the notched-type Gap diode	30
9.	Cross-sectional view of planar-type gap-controlled Schottky diode with applied bias V_A a) voltage dependent depletion region model b) semicircular depletion region model	31
10.	Schematic diagrams of a depletion approximation model for planar-type Gap diodes	35
11.	Schematic of $AsCl_3$ -Ga- H_2 vapor phase epitaxial system	38
12.	Temperature profile of the furnace. Curve (a) is used for the Ga-baking in H_2 and saturation with As of Ga source. Curve (b) is for the epitaxial growth	39

LIST OF FIGURES
(continued)

No.		Page
13.	Doping density as a function of H ₂ S flow rate	46
14.	Cross-section of planar-type gap-controlled GaAs Schottky-barrier diode	50
15.	Carrier concentration versus depth for VPE grown layer from Schottky barrier profile measurements	51
16.	Photograph of 1.5 μm photoresist grating pattern on the GaAs epitaxial layer	53
17.	Process used to fabricate planar-type gap diodes	54
18.	Photographs of 32 μm diameter. Photoresist dots on the aluminum and AuGe/Ni lines	56
19.	Photograph of unalloyed Al/AuGe/Ni stripe dots on GaAs surface after metal etching	58
20.	Completed Gap diodes on a scribed GaAs chip	59
21.	Dimensions of the diode package [35]	60
22.	Photograph of a GaAs Gap diode chip mounted in a C-2 package, bonded with 1 mil Au wires	61
23.	Photographs of various measured low-frequency I-V characteristics of the planar-type diodes as ohmic gap width, W, is gradually increased from zero to more than two depletion widths	63
24.	Photographs of I-V characteristics measured from two typical low-leakage packaged planar-type Gap diodes (Gap diodes U-2, U-5)	64
25.	Photographs of I-V characteristics measured from two wide gap width packaged planar-type Gap diodes (Gap diodes T-9, E-8-B)	66
26.	Photographs of I-V characteristics of a packaged planar-type Gap diode with two different current and voltage scales (Gap diode U-4)	67

LIST OF FIGURES
(continued)

No.		Page
27.	Photographs of I-V characteristics of a packaged planar-type Gap diode with two different current and voltage scales (Gap diode T-3)	68
28.	Representative I-V characteristics of a low-leakage Gap diode and a pure Al Schottky diode of the same size	69
29.	Measures forward I-V characteristics of several Gap diodes and a pure Al Schottky diode	71
30.	Photograph of the temperature dependence of the forward I-V characteristics of a Al Schottky diode measured at four different temperatures	73
31.	Photograph of the temperature dependence of I-V characteristics for a Gap diode	75
32.	Forward I-V characteristics of a pure Schottky diode (UP-5) and a Gap diode (U-2) measured at 21°C and 100°C respectively	76
33.	Photograph of temperature dependence of I-V characteristics of (a) a point contact diode (1N23C) (b) a Gap diode at 22°C, 80°C and 92°C	78
34.	Open-circuit voltage output versus incident RF power for Gap diode (V-10), point contact diode (1N23C) and Schottky diode (UP-4) at 10.565 GHz	79
35.	Open-circuit voltage output versus incident RF power of a Gap diode (V-10)	81
36.	Single-ended mixer conversion loss measuring setup ...	82
37.	Single-ended mixer conversion loss versus local oscillator power for three different Gap diodes (at 10 GHz, 20 MHz IF). The ohmic gap width increases from diode U-3 to diode U-7	84

CONTROL OF GaAs MICROWAVE SCHOTTKY DIODE ELECTRICAL
CHARACTERISTICS BY CONTACT GEOMETRY: THE GAP DIODE

1. INTRODUCTION

Point-contact diodes have been used for many years in mixer and detector applications at microwave frequencies. They are relatively unsophisticated devices consisting of a metal whisker making pressure contact with a semiconductor. In the early 1960's, Schottky-barrier diodes were introduced for similar applications. Schottky diodes have superior noise figure, especially at low IF (Doppler) frequencies, higher burn-out power and better mechanical environmental reliability compared to equivalent point contact diodes [1,2]*.

The GaAs Schottky-barrier diode is preferred to Schottky diodes using other materials owing to its high electron mobility which results in better high frequency performance. Also, both higher and lower temperature operation can be obtained with GaAs owing to its higher energy gap. GaAs Schottky diodes have been shown to have low noise [3]; however, reported barrier heights have been

* The numbers in parentheses in the text indicate references in the Bibliography.

substantially higher than point contact silicon diodes and greater than most silicon Schottky diodes. Barrier heights are related to minimum local oscillator power, the higher barrier devices requiring larger local oscillator power. Therefore, in microwave systems having limited local oscillator power, a low barrier height device is desirable [2,3].

In this report, a new contact technique, which employs conventional Schottky metal contacts separated by ohmic contact gaps to obtain low diode turn-on voltage, is presented. The characteristics of the device made with this new contact configuration, GaAs vapor phase epitaxial growth, and microfabrication technology for the device, together with some microwave measurements, are also described. A discussion of the physics and metallurgy of the metal-semiconductor contact is also presented.

1.1 METAL-SEMICONDUCTOR SCHOTTKY-BARRIER

Metal-semiconductor Schottky-barrier contacts are used in many semiconductor devices, including switches, rectifiers, varactors, IMPATTs, mixer and detector diodes, parametric amplifiers, field effect transistors (MESFETs), and photodetectors. Most of these applications are based on the use of the electron transport properties of the particular metal-semiconductor barrier considered. For each device the design factors depend on the application and may include the metal barrier, semiconductor material, device geometry, passivation, and device packaging.

It is important to study the operation and to optimize the current-voltage characteristic of metal-semiconductor contacts.

Study of such contacts has been pursued since 1938 when Schottky postulated that a potential barrier could arise from a metal-semiconductor interface without the presence of a chemical layer.

1.2 METAL-SEMICONDUCTOR BARRIER HEIGHT

The simple theory of metal-semiconductor contacts [4,5] predicts that the work function of the metal should be a design parameter in controlling the barrier height. Unfortunately, for semiconductors which possess a high surface state density, the barrier height, becomes insensitive to work function. It was first proposed by Bardeen [6] that the influence of a high density of surface states pins the Fermi level at the interface, thus fixing the barrier height. It is experimentally observed that the barrier height for covalent semiconductors is essentially independent of the metal used [7]. Like the group IV semiconductors Si and Ge, GaAs and most of the other III-V compound semiconductors are highly covalent. For highly ionic materials such as most of the II-VI compound semiconductors (e.g. ZnS and ZnO) and the transition-metal oxides, the barrier height is strongly dependent on the work function of the metal [7].

The electric field and potential resulting from surface states in the Schottky-barrier depletion region is shown in Figure 1. Figure 2 shows experimental data on barrier height, ϕ_B , for a range of metals on n-type Si, GaAs, GaP and CdS [4]. The ability to vary ϕ_B for different applications is important for device optimization. For example, in a mixer diode the capability of the device to handle low signal levels without d.c. bias requires low turn-on voltage. Consequently, a mixer or detector diode requires a low barrier

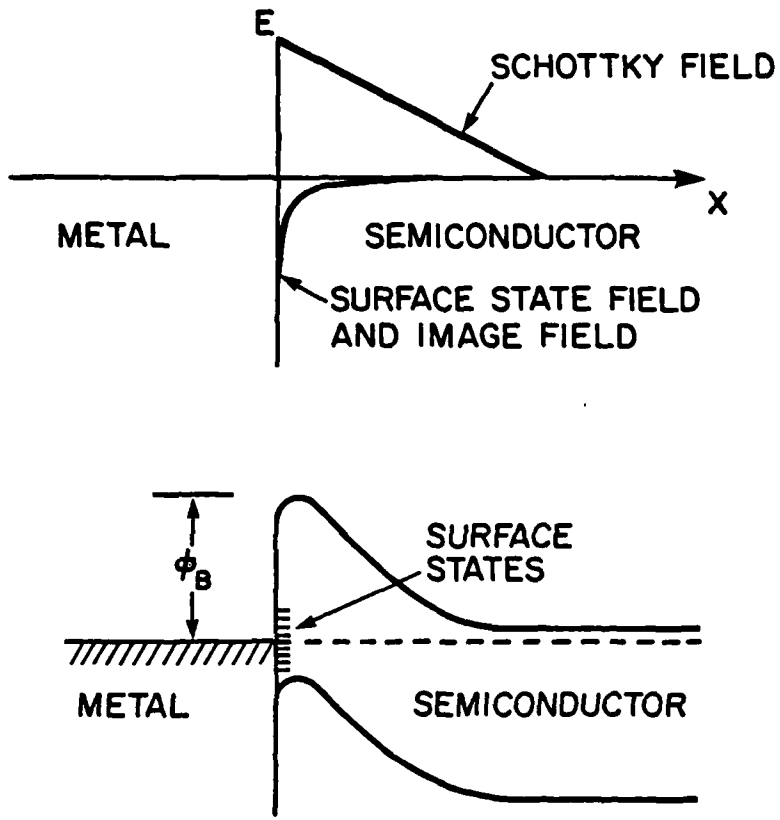


Figure 1. Schematic representation of electric field and potential resulting from surface states in the Schottky-barrier depletion region

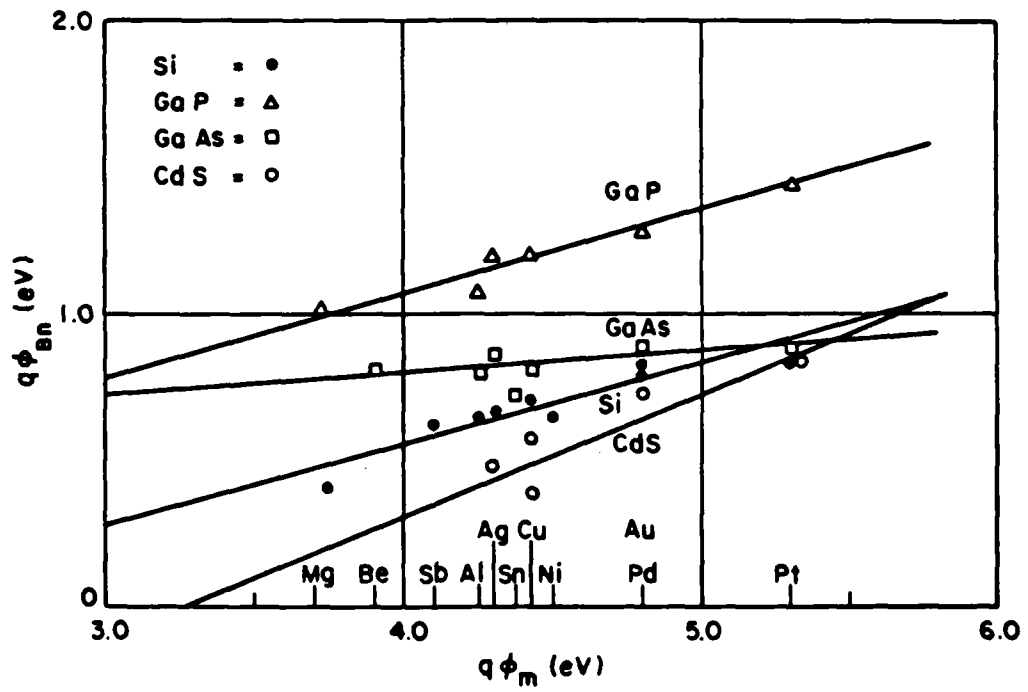


Figure 2. Experimental barrier heights for metal contacts to n-type Si, GaAs, GaP and CdS [4]

height that will yield a low forward voltage drop. For this reason the point contact diode has traditionally been preferred to the evaporated Schottky diode. A mixer also requires low series resistance for high conversion efficiency. Therefore GaAs is preferred to silicon because the high mobility of the undepleted material is more important than its high contact potential, about 0.8 ev.

1.3 CONTROL OF BARRIER HEIGHT

There are several techniques available for varying the effective barrier height of metal contacts to materials with high surface state densities. An introduction of these techniques is made in the following sections. The barrier height may be used as a design parameter for Schottky diodes with the aid of barrier variation techniques.

1.3.1 Highly Electronegative Contacts [8]

It is seen in Figure 1 that the insensitivity of the barrier height to the electronegativity of the contact metal in semiconductors with high surface state densities prevents the use of intrinsic barrier height as a control parameter. Attempts to overcome this problem for II-VI and III-V compound semiconductors have led to some developments in the use of highly electronegative metallic compounds, rather than elemental metal materials, such as polymeric sulfur nitride $(\text{SN})_x$ and the mercury chalcogenides to extend the available range of Schottky barrier heights [8]. These metallic compounds produce higher barriers to n-type semiconductors and lower barriers to p-type semiconductors than do the elemental metals. For example, studies of the use of the $(\text{SN})_x$ compounds on

n-type GaAs and InP indicate that the Schottky-barrier heights are increased by 0.1 eV and 0.3 eV respectively, compared to those obtained with Au [8].

1.3.2 Doping Variations Near the Contact [9]

As the carrier concentration of a semiconductor is increased, the depletion width under the Schottky contact decreases and the surface field increases. With the increased doping, the dominant transport mechanism across the barrier can change from thermionic emission to thermionic field emission [4]. Therefore, the effective barrier height of a Schottky-barrier having a highly doped surface layer can be controlled over a wide range. Reduction of barrier height is effected by increasing the surface field and encouraging quantum-mechanical tunneling through the barrier; increase of barrier height occurs when the surface field is reversed. In practice, the semiconductor can be made degenerate which results in an ohmic contact.

1.3.2.1 Alloying [10,11,12]

A simple way to achieve local variation in doping is to alloy the contact. The dopant is diffused into the semiconductor. For materials such as GaAs and InP the contact metal is usually a mixture of elements such as AuGe or AgSn, where Ge or Sn is used as a dopant. Also a single-component metal Schottky-barrier can be heated to produce interdiffusion at the interface. For example, the heating of a Au/GaAs barrier to 450°C results in a reduction of the effective barrier height from 0.95 to 0.48 eV [12].

The basis for either alloying technology is empirical and not very reproducible. One of the problems of the alloying process described above is nonuniformity, due to the incomplete removal of residual surface oxides prior to the evaporation of the metal contact.

1.3.2.2 Ion Implantation [13,14]

Ion implantation is a technique that can be more controllable than the means described above for modifying the effective barrier height, because the depth and surface density of the implanted impurity can be controlled accurately by adjusting the energy of the implant. The implantation of donors into n-type material, followed by the usual annealing procedure to reduce the damage and activate the dopants, can be used to reduce the effective barrier height [14].

1.3.2.3 Ion Bombardment [15]

Semiconductor defects resulting from ion bombardment can be used instead of implanted dopants, to change the effective barrier height. Consider a metal-semiconductor junction. If deep levels are introduced into the semiconductor near the interface, the surface state density will increase and the valence band will bend downward at the interface as shown in Figure 1.

1.3.3 Thin Interfacial Insulating Layers [16,17,18]

Thin interfacial oxide films can have a strong effect on terminal I-V and C-V characteristics. Published experimental results on Si, GaAs and InP reveal that the use of interfacial layers is beginning to prove a valuable addition to Schottky barrier technology.

1.3.4 Edge Tunneling [19]

As the diameter of a planar Schottky-barrier device is reduced, the depletion region at the circumference of the metal contact narrows, and the thermionic field emission (tunnelling) current component increases, resulting in a decrease in the effective barrier height. This high edge field tunnelling phenomenon is the reason why point contact diodes have a low turn-on voltage.

1.3.5 Gap-Controlled Low Barrier

When the applied voltage varies, the depth of the high resistivity depletion region of the Schottky-barrier also varies. If ohmic contact gaps are opened in the Schottky-barrier, then the current-voltage characteristic of the resulting device can be modulated by varying the configuration of the ohmic contact openings.

This report describes the investigation of this new barrier lowering technique. GaAs Schottky-barrier diodes, combined with AuGe/Ni ohmic contacts, have been fabricated and used to detect signals at microwave frequencies. Depending on the width of the ohmic contact gaps, the experimental diodes exhibit either high efficiency microwave detection or low turn-on Schottky-barrier mixers requiring low RF local oscillator power comparable to that of point contact diodes.

Chapter 2 describes the principle of operation of the Gap diode and presents some approximate theory for the current-voltage relationship for two different types of Gap diodes. The design of a GaAs epitaxial growth reactor and growth techniques are described in Chapter 3, while Chapter 4 presents the technology used to fabricate

experimental GaAs Gap diodes. Device characteristics and RF performance are reported in Chapter 5. Our results are summarized and recommendations for future work are presented in Chapter 6.

2. GAP-CONTROLLED LOW-BARRIER SCHOTTKY DIODE

In this chapter the physics of the Schottky barrier junctions is reviewed and the principle of operation of the Gap diode is explored. Prediction of the device I-V characteristics are developed.

2.1 SCHOTTKY-BARRIER MODEL

Schottky's diffusion theory [20] in an intimate metal-semiconductor contact postulates the existence of a space charge region which gives rise to an electrostatic potential energy barrier. The space charge region, which is depleted of mobile carriers, is situated in the semiconductor adjacent to the metal layer. The analytical description of the barrier yields the relationship between the applied bias, barrier height, donor concentration and energy band bending in the semiconductor. In the absence of image force rounding and assuming that the ionized impurities are uniformly distributed in the semiconductor, the one-dimensional parabolic potential energy barrier in the semiconductor depletion region, shown in Figure 3, is described by

$$\phi(x) = \frac{q^2 N_D x^2}{2\epsilon_s \epsilon_0} \quad (2.1)$$

for $0 \leq x \leq d$

Here q is the electronic charge, N_D is the ionized donor concentration, ϵ_s is the static dielectric constant, and ϵ_0 the permittivity

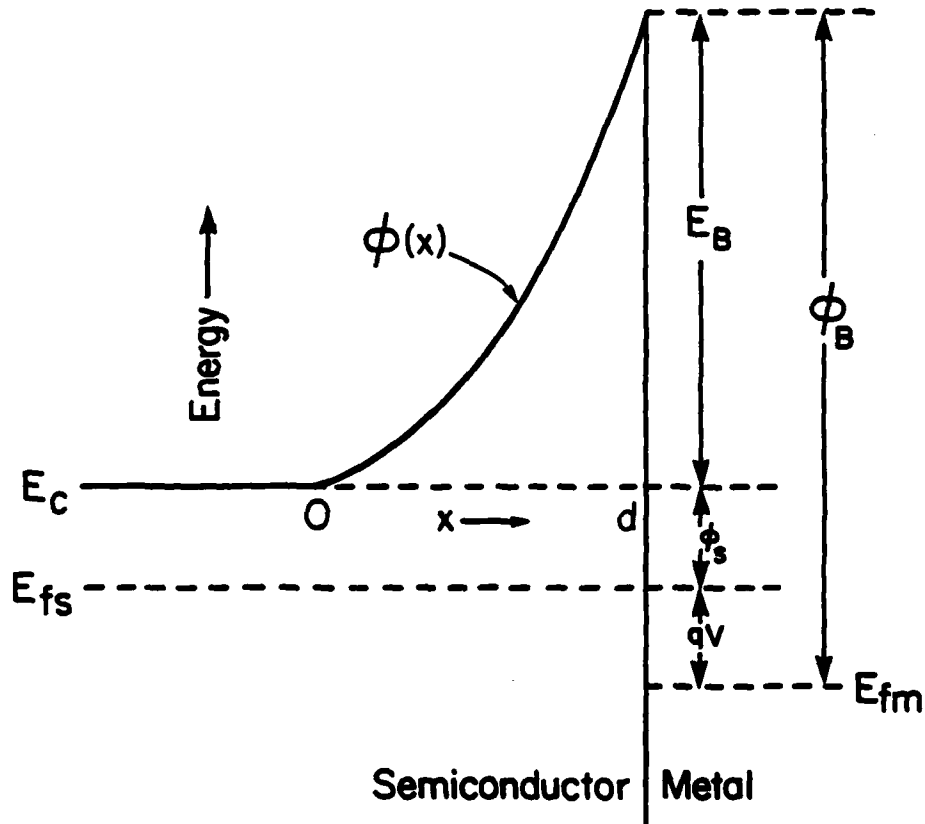


Figure 3. One-dimensional parabolic depletion layer potential energy barrier for an n-type semiconductor. Image force rounding of the barrier shape is neglected

of free space. The depletion layer width, d is related to the energy band bending in the depletion region, E_B , by

$$E_B = \phi_B - \phi_s - qV = \frac{q^2 N_D d^2}{2\epsilon_s \epsilon_0} \quad (2.2)$$

where ϕ_B is the metal-semiconductor barrier height, ϕ_s the position of the semiconductor Fermi level relative to the conduction band edge, and V the applied bias.

Depending on the difference of work function between the semiconductor and metal, three other configurations are possible: a depletion layer barrier for p-type semiconductor, and accumulation layers (ohmic contact) for n or p-type material.

For low-doped Schottky-barrier diodes, using Maxwell-Boltzmann statistics to describe the distribution of carriers that can be emitted over the barrier, one can relate the forward carrier flux J_f and reverse carrier flux J_r by

$$J_f = J_r \exp\left(\frac{qV}{kT}\right) \quad (2.3)$$

where $J_r = A^* T^2 \exp\left(\frac{-q\phi_B}{kT}\right)$ (2.4)

Here, A^* is the Richardson constant of the semiconductor [21], k is Boltzmann's constant and T the absolute temperature. The total current density can be written as:

$$\begin{aligned}
 J &= J_f - J_r = J_r \left[\exp \left(\frac{qV}{kT} \right) - 1 \right] \\
 &= A^* T^2 \exp \left(\frac{-q\phi_B}{kT} \right) \left[\exp \left(\frac{qV}{kT} \right) - 1 \right] \quad (2.5)
 \end{aligned}$$

which represents ideal thermionic emission over the barrier. The diode equation derived from the Schottky's diffusion theory [20] yields a bias dependent pre-exponential term different from A^*T^2 .

In reality, the shape of the potential barrier is not parabolic because charge carriers in the semiconductor are electrostatically attracted towards the metal by an induced mirror image charge of opposite sign in the metal. The image force effect changes the potential distribution to

$$\phi(x) = \frac{q^2 N_D x^2}{2\epsilon_s \epsilon_0} - \frac{q^2}{16\pi\epsilon_d \epsilon_0 (d-x)} \quad (2.6)$$

where ϵ_d is the relative dynamic dielectric constant of the semiconductor [22].

The lowering of the barrier due to the image effect is given by [23]

$$\Delta\phi = \left(\frac{q^2 E_B N_D}{8\pi^2 \epsilon_s \epsilon_d^2 \epsilon_0^3} \right)^{\frac{1}{4}} \quad (2.7)$$

Therefore, as the donor concentration, N_D , of the semiconductor is increased, the depletion width narrowing ($d \propto N_D^{-1/2}$) proceeds more rapidly than the potential barrier lowering ($\Delta\phi \propto N_D^{1/4}$) and,

consequently, the carrier transport is dominated by quantum-mechanical tunneling rather than by thermionic emission through the barrier. Because of the image force effect, the actual barrier height is $\phi_B - \Delta\phi$ where $\Delta\phi$ is bias dependent (see Equations (2.2) and (2.7)).

For materials doped with $N_D \lesssim 10^{17} \text{ cm}^{-3}$, thermionic emission of carriers gives rise to current rectification in Schottky barriers. There are two other modes of carrier transport over the Schottky barrier that involve tunneling effects. As the impurity concentration of the semiconductor is increased ($N_D \approx 10^{18} - 10^{19} \text{ cm}^{-3}$), initially, the barrier becomes thin enough that thermally excited carriers can tunnel through near the top of the barrier. This mode of carrier transport is referred to as thermionic field emission or thermally-assisted tunneling, which is temperature dependent.

As the impurity concentration is increased even further ($N_D \geq 10^{19} \text{ cm}^{-3}$), the barrier width becomes so thin that significant numbers of carriers can tunnel through even at the base of the barrier. This mode is called field emission tunneling and is temperature independent. The mechanism of metal-semiconductor ohmic contacts is based on this mode of carrier transport.

Because of the image force lowering, and the presence of inevitable surface states and interfacial dielectric layers between the metal and semiconductor, a dimensionless empirical factor n is introduced in the diode equation in order to allow

for deviation from ideality. The current, I , of the Schottky-barrier is related to the applied voltage, V , by the expression

$$I = I_s \left[\exp\left(\frac{qV}{nKT}\right) - 1 \right] \quad (2.8)$$

where $I_s = S' A^{**} T^2 \exp\left(\frac{-q\phi_B}{KT}\right)$ (2.9)

I_s is the saturation current

S' is the area of the diode

The ideality factor, n , is a function of temperature, and is determined from the slope of linear plots of $\ln I$ against V . The slope of the forward characteristic is measured for $V \gg \frac{3nKT}{q}$. I_s is determined by the extrapolation from higher forward bias voltage to zero voltage of the $\ln I$ versus V plot.

2.2 OHMIC CONTACT TO GaAs [7,10,24,25,26]

The most common method of making an ohmic contact is to place a metal layer in contact with a semiconductor surface of very high doping, to achieve field-emission dominated carrier transport so that the potential barrier will appear almost transparent to the carrier flow. There are many ways to make such a highly doped surface layer such as alloy regrowth, diffusion of dopant contained in the contact material, epitaxial regrowth, or ion implantation.

For the alloy regrowth technique, the metal dissolves some of the semiconductor during heating. Upon cooling the dissolved

semiconductor will regrow on the underlying crystal. The regrown layer will contain a substantial concentration of the metal which acts as a dopant (e.g. Au - n GaAs). If higher doping level and lower alloying temperature are required it is often advantageous to utilize another dopant impurity in addition to the contact metal (e.g. Au-Ge-n GaAs).

The ohmic contact used for the fabrication of the Gap diode in this report is the widely used Ni/Au-Ge/n-GaAs alloyed contact [25,26]. The explanation for this ohmic behaviour is that the diffused Ge atoms occupy Ga vacancies during alloying and form a n^+ layer, sufficiently heavily doped to produce a linear current-voltage characteristic at the contact interface. Ni plays an active role in the contact formation. Wittmer, et al. [25] have shown experimentally that during heat treatment the Ge diffuses out of the Au into the Ni layer and forms stable compounds. The Ni layer acts as a sink for Ge and the uniformity of the alloyed layers depend on the ratio of the amount of the evaporated Ge to Ni. From Auger electron spectroscopy (AES), it is known that the Ni does not remain on top of the Au-Ge layer but it moves rapidly under the Au-Ge layer before the Au-Ge melting point is reached [26]. The reason for the improvement in surface uniformity due to the inclusion of Ni is that the presence of Ni at the GaAs surface greatly improves the wetting of liquid Au-Ge to GaAs.

2.3 THEORY OF GAP-CONTROLLED CHARGE TRANSPORT

2.3.1 Basic Characteristics

In a conventional Schottky-barrier diode charge carriers must surmount the potential barrier at the metal-semiconductor interface to contribute to the current. An exponential relation between the applied voltage and the current results. Another means of obtaining a voltage controlled current is conductivity modulation, as for example, in the Field Effect transistor. This process can be used to make a diode whose performance will be markedly different from that of the conventional Schottky-barrier diode.

Consider what happens if a gap is opened in the Schottky metal on the surface of an n-type epitaxial layer, thus exposing the underlying n-layer. Now an ohmic metallization is applied to the entire surface. This forms an ohmic contact to the n-layer and connects it and the separated Schottky contacts in parallel.

Two types of Gap diodes are shown in Figures 4a and 4b, one with the Schottky metal on the upper surface, the other with the metal deposited into notches extending below the surface. The device comprises an n-type layer grown epitaxially on a heavily doped n^+ substrate with an ohmic contact fabricated on the substrate side of the wafer. The diode consists of a conductive channel with an ohmic contact on top, provided with two Schottky-barrier contacts acting as gates to control the conductance of the conductive channel. Thus the gap-controlled Schottky is basically an intrinsic-biased voltage-controlled resistor whose resistance can be varied with the width of

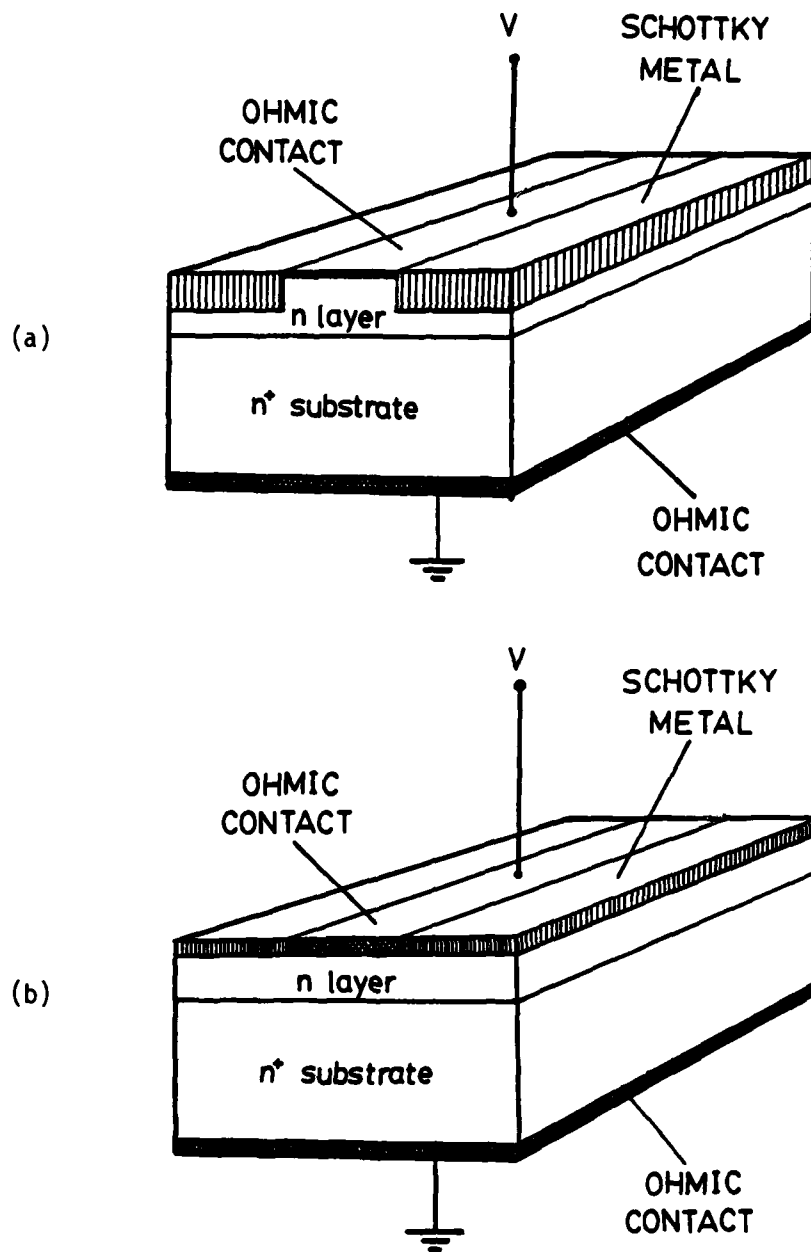


Figure 4. Schematic diagram of gap-controlled Schottky Diode
(a) notched type (b) planar-type

the depleted space-charge region extending into the channel. Current is transported predominantly by electrons only.

The potential distribution in the barrier layer of a metal-n-type semiconductor can be calculated by solving Poisson's equation, proceeding in the same manner as for the abrupt p-n junction. Under the abrupt junction approximation, the depletion width, d , of the barrier layer can be expressed as

$$d = \sqrt{\frac{2\epsilon_s \epsilon_0}{qN_D} (V_0 - V)} \quad (2.10)$$

where V_0 is the diffusion potential or built-in voltage of the metal-semiconductor junction, V the applied voltage, and N_D the donor concentration.

The space-charge density ρ of the semiconductor is

$$\rho = q(N_D - n) \quad (2.11)$$

where n is free electron concentration. Inside the depletion region, $\rho \approx qN_D$, $x < d$. In the neutral region the potential is constant, that is $\frac{dV}{dx} \approx 0$, $\rho=0$, $n=N_D$, $x > d$. This is the depletion approximation.

If the image force effect is included, the depletion width of the semiconductor in thermal equilibrium may be written as [4]

$$d = \sqrt{\frac{2\epsilon_s \epsilon_0}{qN_D} (\phi_{Bn} + \Delta\phi - V - \frac{KT}{q})} \quad (2.12)$$

where ϕ_{Bn} is the metal-semiconductor barrier height and $\Delta\phi$ is the image force barrier lowering. The term $\frac{KT}{q}$ arises from the contribution of mobile carriers to the electric field in the depletion region.

In Figure 5, we illustrate the condition with an applied bias $V = V_A$. If a small positive voltage is applied to the metal the depleted region separate and a current will be conducted through the n-type channel between the ohmic contacts. No charge flows in the depletion regions. As the voltage is increased, the width of the undepleted channel grows and the channel conductance increases. The I-V characteristic is not linear and is determined by the structure of the diode. As the applied positive voltage is further increased beyond the turn-on voltage of the Schottky-barrier, another current component will arise due to charges flowing through the Schottky-barriers. Thus the current of the diode consists of two components:

$$I \text{ (Total current)} = I_1 \text{ (current through the ohmic region)} \\ + I_2 \text{ (current through the Schottky barrier)} \quad (2.13)$$

In the reverse-bias case, when negative voltage is applied to the metal, the depletion width is increased. This restricts current conduction through a smaller channel cross-sectional area. Thus the channel resistance is increased. As the reverse bias is further increased, the enlarged depletion regions will eventually touch in the channel near the substrate

side. This happens when the ohmic gap width $W = 2d$. Using Equation (2.10), the corresponding applied voltage may be expressed as

$$V_{\text{sat}} = \frac{qN_D W^2}{8\epsilon_s \epsilon_0} - V_0 \quad (2.14)$$

At this saturation voltage, V_{sat} , the channel is completely depleted and normally does not conduct because there are very few carriers in it. However, similar to the field-effect transistor, a current will still be conducted through the diode by drift of carriers from the ohmic contact due to the high applied field. Generally, the phenomenon is called saturation because the reverse current saturates with increasing applied voltage.

By choosing appropriate configurations of ohmic and Schottky metal contacts, the turn-on voltage of the diode can be reduced to a value below the built-in voltage without significant degradation of the reverse leakage current. However, if the series resistance of the Gap diode is made small, the reverse-bias current is unlikely to be saturated similar to the situation of the vertical junction field-effect transistor [27].

Two-dimensional numerical analysis may be applied to the Gap diode, with suitable metal-semiconductor boundary conditions, to obtain current-voltage characteristics of the diode. In the following sections, an approximate theory for the current-voltage characteristics for the Gap diode is derived, based on the abrupt depletion approximation and constant mobility assumption

at low bias. These I-V characteristics may be used in first order design considerations for the Gap diode.

2.3.2 Current-Voltage Characteristic

2.3.2.1 Notched-Type Gap Diode

Let us consider the notched gap-controlled Schottky diode shown in Figure 4a, with an applied voltage V_A , before the onset of the saturation (depletion region pinched-off). The cross-sectional view of the device is shown in Figure 5.

The basic dimensions of the device are gap width W , channel width S , and Schottky metal thickness (channel length) ℓ . In this analysis W is larger than two zero-bias depletion widths. The quantity $d(y)$ is the depletion width along the channel. The substrate electrode is grounded.

Consider the non-pinched-off low-bias situation. The current is carried mainly through the ohmic channel and the voltage drop of the applied voltage V_A will be across the undepleted region in the channel.

The resistance of the channel is given by

$$R = \frac{\ell}{q\mu_n N_D S(W-2d)} \quad (2.15)$$

where we have taken the depletion width d constant along the channel; μ_n is the mobility of the semiconductor. Because the voltage drops along the channel (in the y -direction), the depletion width, d , along the channel will be a function of the applied voltage.

The elemental voltage drop dV_y along the channel is written as

$$dV_y = \frac{I_A dy}{q\mu_n N_D S [W - 2d(y)]} \quad (2.16)$$

where I_A is the total current through the channel. It is assumed that there is no current flowing through the Schottky metal at small applied bias. The depletion width $d(y)$ at position y is given by

$$d(y) = \sqrt{\frac{2\epsilon_s \epsilon_0 [V_0 - (V_A - V_y)]}{q N_D}} \quad (2.17)$$

where V_y is the voltage at position y in the channel. It is a good approximation to assume the boundary condition for the voltage drop as

$$V_y = \begin{cases} 0 & , \quad y=0 \\ V_A & , \quad y=\ell \end{cases} \quad (2.18)$$

This analysis neglects the series resistance between $y=0$ and the substrate.

Substituting Equation (2.17) into Equation (2.16) and integrating between $y=0$, $V=0$ and $y=\ell$, $V=V_A$ leads to the current-voltage relationship of the notched-type gap-controlled diode:

$$I_A = \frac{q\mu_n N_D S}{\ell} \left\{ W V_A - \frac{4}{3} \sqrt{\frac{2\epsilon_s \epsilon_0}{qN_D}} [V_o^{\frac{3}{2}} - (V_o - V_A)^{\frac{3}{2}}] \right\} \quad (2.19)$$

or

$$I_A = \frac{1}{R_o} \left\{ V_A - \frac{4}{3} \sqrt{\frac{2\epsilon_s \epsilon_0}{W^2 qN_D}} [V_o^{\frac{3}{2}} - (V_o - V_A)^{\frac{3}{2}}] \right\} \quad (2.20)$$

where

$$R_o = \frac{\ell}{q\mu_n N_D S W} \quad (2.21)$$

is the resistance of the channel when there is no Schottky metal or depletion region.

This idealized current-voltage relationship for the notched-type Gap diode is derived under the assumptions of the abrupt depletion approximation and constant mobility of the semiconductor. It may be used as a first order estimate of the turn-on voltage and I-V characteristics of the Gap diode.

Figure 6 shows the calculated current-voltage characteristics of GaAs notched-type Gap diode from Equation (2.19) as a function of ohmic gap width, W. The configuration and semiconductor parameters used for this calculation is also shown there. If the turn-on voltage of the diode is defined at a specific current value, then the calculated relationship of the turn-on voltage V_{on} , ohmic gap width W and semiconductor carrier concentration N_D is shown in Figure 7.

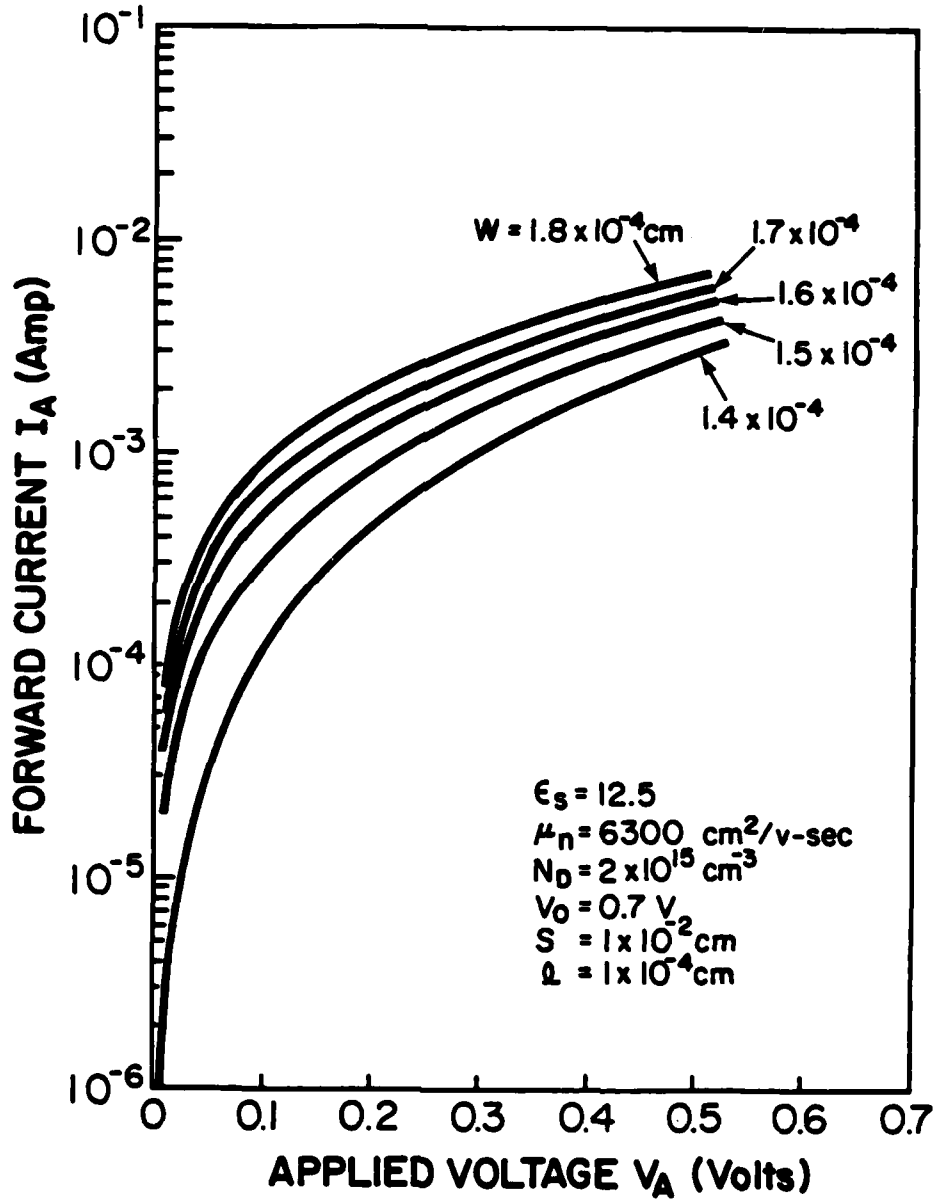


Figure 6.

Calculated forward I-V characteristics of the notched-type Gap diode from Equation (2.19) as a function of ohmic gap width W

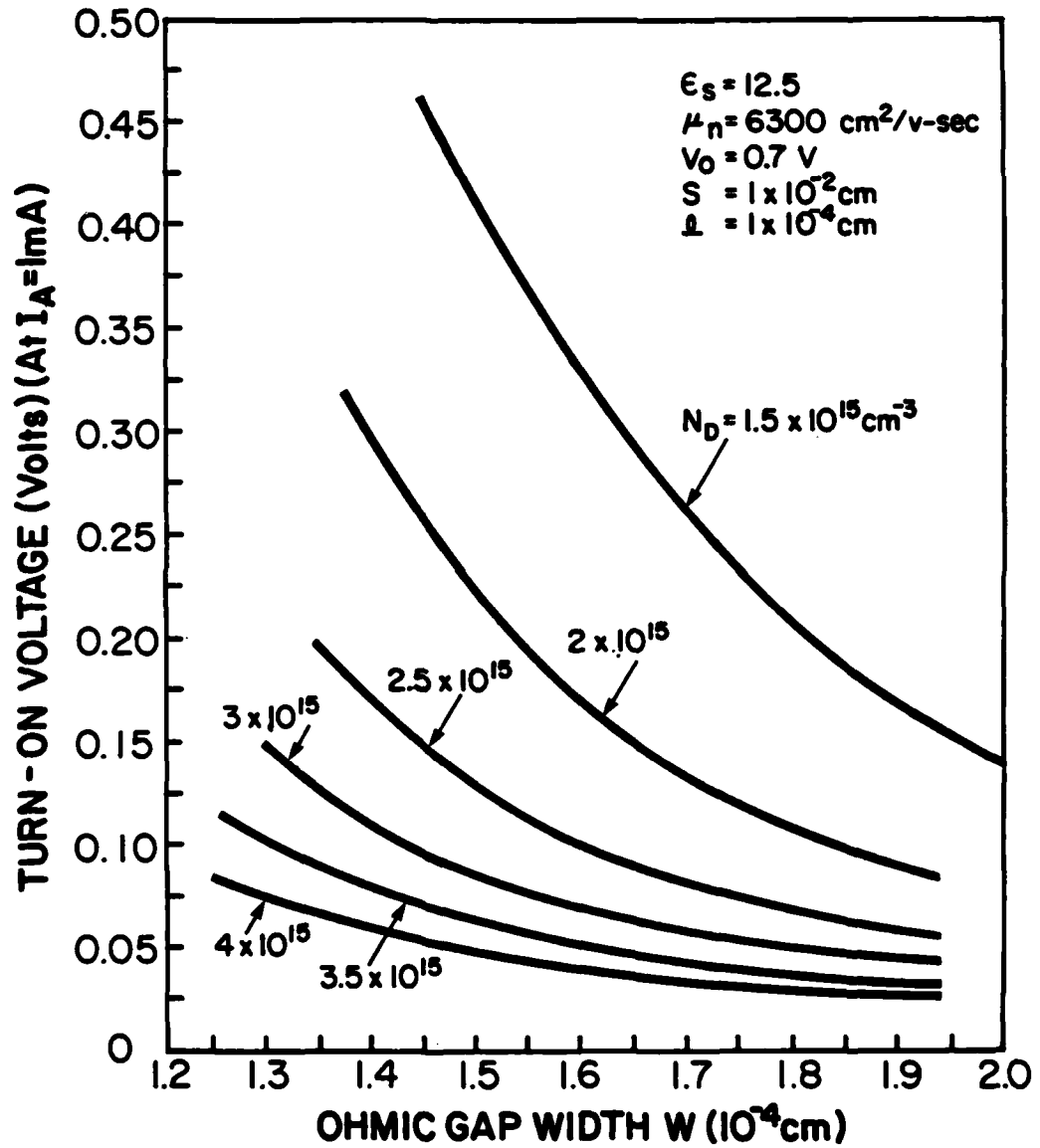


Figure 7.

Calculated relationship between the turn-on voltage (at $I_A = 1$ mA), ohmic gap width W and semiconductor carrier concentration N_D of the notched-type Gap diode

For efficient detector or low LO-power mixer applications, a high reverse resistance and a low forward resistance near the origin are desirable. The cut-off frequency of the diode is inversely proportional to the diode series resistance and capacitance. When the applied voltage is less than the turn-on voltage of the Schottky metal, the series resistance of the gap diode is proportional to the diode channel length ℓ . The calculated relationship between the turn-on voltage (at $I_A=1$ mA) and ohmic gap width W and semiconductor channel length ℓ is shown in Figure 8.

In the analysis of the notched-type diode the depletion width just below the ohmic region ($y=\ell$) remains constant because the potential at the Schottky metal and ohmic contact are the same. Therefore, if the channel length, ℓ , of the diode is large, the diode forward current will be limited by a large series resistance prior to the turn-on voltage of the Schottky metal. However, the advantage of the long channel Gap diode is that the reverse leakage current is small, because the depletion regions in the channel are pinched off tightly.

For high frequency applications, a shorter charge transition region is desirable. This requires shorter channel length. Therefore, the planar-type Gap diode with channel length, ℓ , equal to zero is proposed in the following section. The experimental results of Chapter 5 are based on this type of Gap diode.

2.3.2.2 Planar-Type Gap Diode

Figures 9a and 9b show schematic diagrams of two different depletion approximations for the planar type gap-controlled diode. Current-voltage relations are derived based on two different

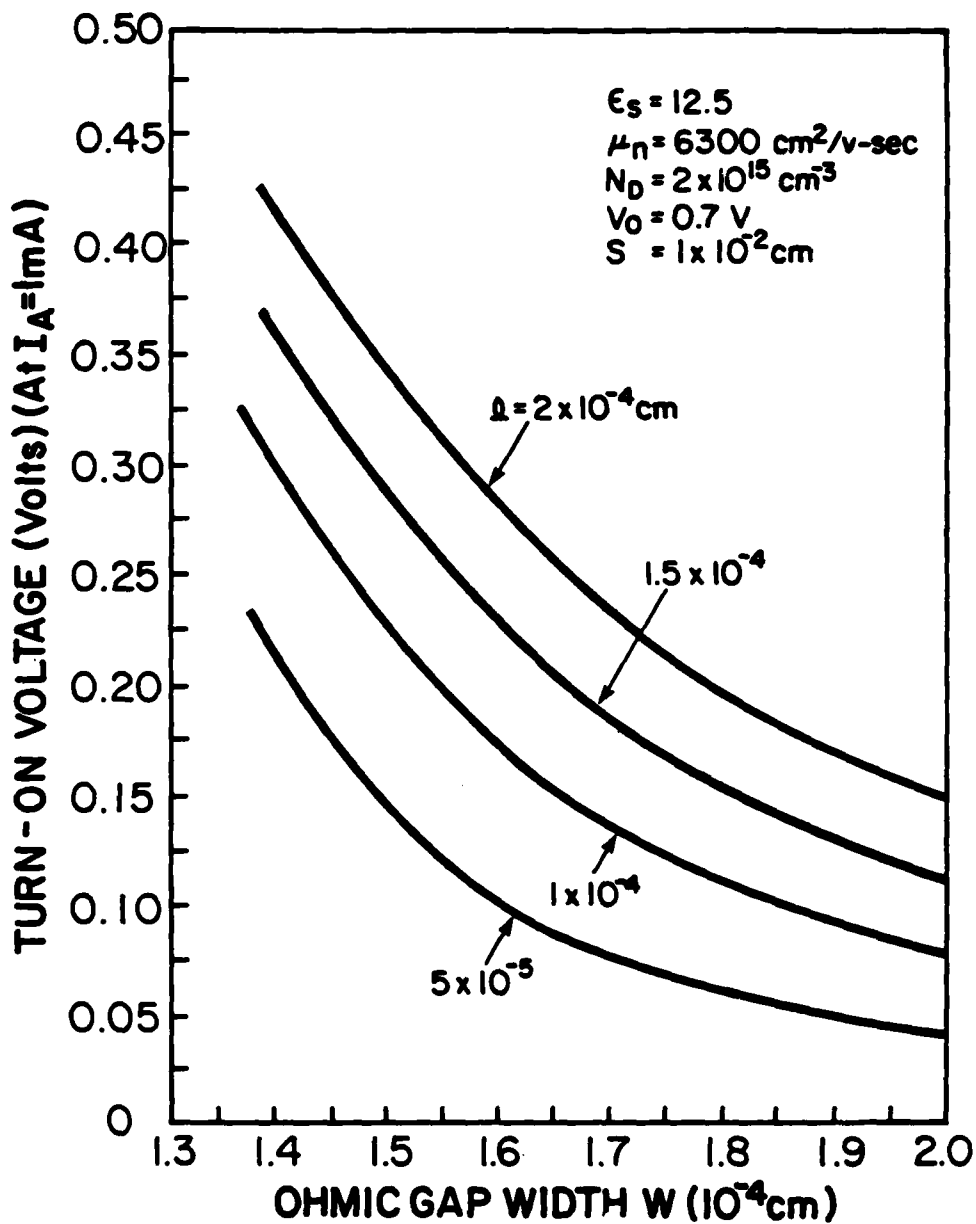


Figure 8. Calculated relationship between the turn-on voltage (at $I_A = 1 \text{ mA}$), ohmic gap width W and semiconductor channel length l of the notched-type Gap diode

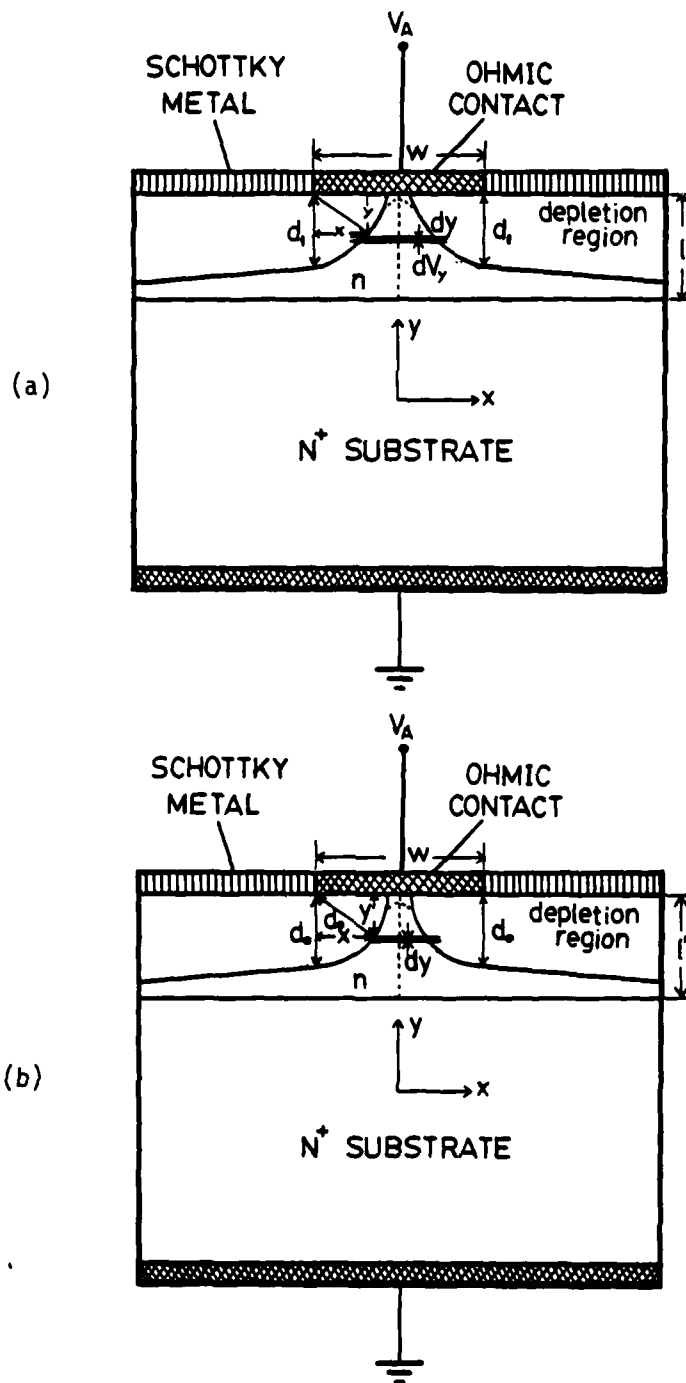


Figure 9. Cross-sectional view of planar-type gap-controlled Schottky diode with applied bias V_A
a) voltage dependent depletion region model
b) semicircular depletion region model

assumptions. The first case considers that the applied voltage drops along the channel as is shown in Figure 9a. The depletion depth under the ohmic contact edge is assumed smaller than that under the Schottky metal and is given by

$$d_1 = \sqrt{\frac{\epsilon_s \epsilon_0}{q N_D} (V_0 - V_A)} \quad (2.22)$$

where V_A is applied voltage.

The elemental voltage drop along the channel can be written as

$$dV_y = \frac{I_A dy}{q \mu_n N_D S (W - 2X)} \quad (2.23)$$

where

$$X \approx \sqrt{\frac{\epsilon_s \epsilon_0}{q N_D} (V_0 - V_A + V_y)} \times \left(\frac{V_y}{V_A}\right) \quad (2.24)$$

Equation (2.24) is an approximate relation taken in order to match the boundary conditions which for Equations (2.22) (2.23) are:

$$V_y = \begin{cases} 0 & , & y=0 \\ V_A & , & y=d_1 \end{cases}$$

Substituting Equation (2.24) into Equation (2.23) and integrating between $y=0$ and $y=d_1$ leads to the approximate current-voltage relationship of the planar gap-controlled diode:

$$I_A \approx \frac{4q\mu_n N_D S}{V_A \sqrt{V_0 - V_A}} \left\{ \frac{1}{5} [(V_0 - V_A)^{\frac{5}{2}} - V_0^{\frac{5}{2}}] - \frac{V_0 - V_A}{3} [(V_0 - V_A)^{\frac{3}{2}} - V_0^{\frac{3}{2}}] \right\} + \frac{d_1 V_A W}{q\mu_n N_D S} \quad (2.25)$$

The series resistance below the channel region is omitted in this calculation.

The turn-on voltage of the planar-type gap diode will be lower than that of the notched-type Gap diode, because the depletion regions are not pinched off tightly. Likewise, the reverse isolation is worse in the planar-type diode. The optimum configuration for low turn-on voltage, small reverse leakage current of the Gap diode will be something between the notched and planar-types.

Figure 9b is a schematic of another simple depletion approximation for the planar type diode. It is assumed here that the depletion width under the ohmic region decreases as the applied voltage increases and is independent of the voltage drop along the channel. The shape of the depletion edge and depletion depth are assured as follows:

$$x = \sqrt{d_0^2 - y^2} \quad (2.26)$$

and

$$d_0 = \sqrt{\frac{2\epsilon_s \epsilon_0}{qN_D} (V_0 - V_A)} \quad (2.27)$$

The diode current may be written as

$$I_A = \frac{V_A}{\int_0^{d_0} \frac{dy}{q\mu_n N_D S (W - 2\sqrt{d_0^2 - y^2})} + \frac{\ell' - d_0}{WSF \times q\mu_n N_D}} \quad (2.28)$$

where ℓ' is the thickness of the epitaxial layer. The series resistance under the channel region is taken into consideration and F is a number larger than one which is used as a factor to obtain the approximate cross-section area for the series resistance.

The integration in Equation (2.28) can be evaluated analytically and the current expression can be written as

$$I_A = \frac{V_A}{\frac{1}{2q\mu_n N_D S} \left[\frac{-\pi}{2} + \frac{2K}{\sqrt{K^2 - 1}} \tan^{-1} \sqrt{\frac{K+1}{K-1}} \right] + \frac{\ell' - d_0}{q\mu_n N_D W S F}} \quad (2.29)$$

where

$$K = \frac{W}{2d_0}$$

Equation (2.29) is an crude current-voltage approximation which may be used to estimate the diode turn-on voltage and I-V characteristics of the diode. The forward current will increase faster than that of the preceding method.

Figure 10 shows schematic diagrams of the depletion approximation model for a planar-type Gap diode under (a) forward bias (b) zero bias and (c) reverse bias conditions. In the diagram the depletion

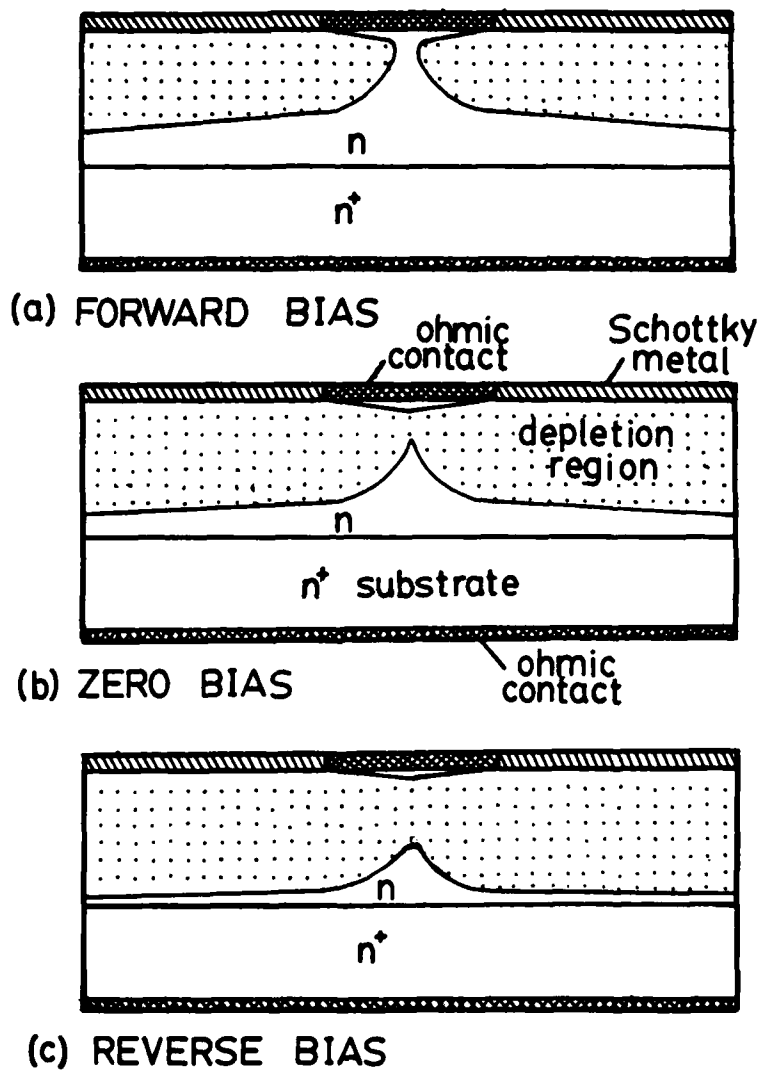


Figure 10. Schematic diagrams of a depletion approximation model for planar-type Gap diodes

region is pinched-off slightly under zero bias. Therefore, the reverse current isolation is improved at the expense of high turn-on voltage. A good diode is a unidirectional device with efficient rectification, hence high reverse leakage will degrade the performance of the diode drastically. Fabrication technology and experimental results of the planar-type Gap diode are presented in the following chapters.

3. VAPOR PHASE EPITAXIAL GROWTH OF GaAs

In this chapter we describe the epitaxial reactor and techniques employed for the growth of GaAs layers used in Gap diode fabrication.

3.1 DESCRIPTION OF EPITAXIAL REACTOR

GaAs epitaxial layers are grown in an AsCl_3 -Ga- H_2 flow system of the type first described by Knight et al. [28]. A schematic diagram of the reactor and two-zone furnace is shown in Figure 11. This appears to be intrinsically a simple and reliable system and has the advantage over other systems that all the starting reagents are obtainable in a state of high purity. Efforts have been directed, first, to reducing impurities in the system, and second, to controlling physical growth processes which cause variations in electrical properties.

The two-zone furnace has two independent temperature controllers. The temperature profile of the furnace is shown in Figure 12. The reactor tube, seed holder and melt boat are constructed of quartz. All the gas lines up to the flow valves, except the aluminum H_2S dopant line, are stainless steel. The AsCl_3 bubbler is constructed of Pyrex and cooled by a constant temperature refrigerated circulator attached to the water bath.

The furnace is mounted on a wheeled stage so that it can be moved along the reaction tube to heat or cool the reactor quickly, thereby shortening the exposure time of the arsenic-saturated Ga source under the hot hydrogen flow before and after the growth time. Dissolution of GaAs crusted over the Ga source was observed when it was exposed

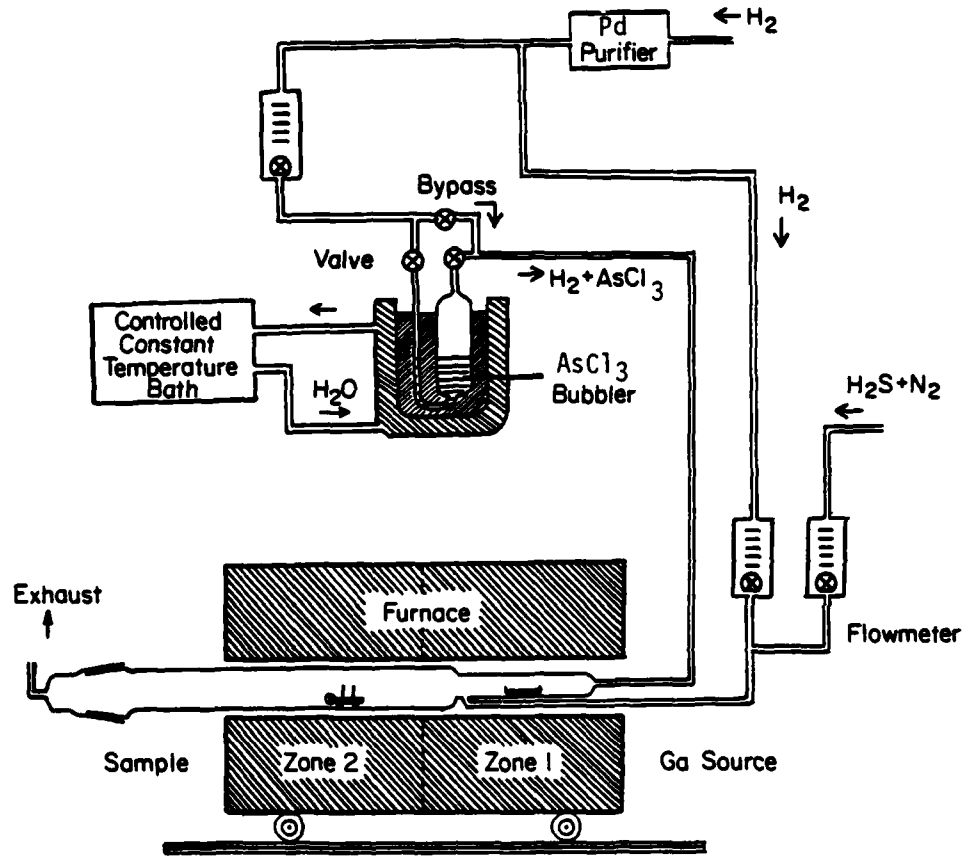


Figure 11. Schematic of AsCl₃-Ga-H₂ vapor phase epitaxial system

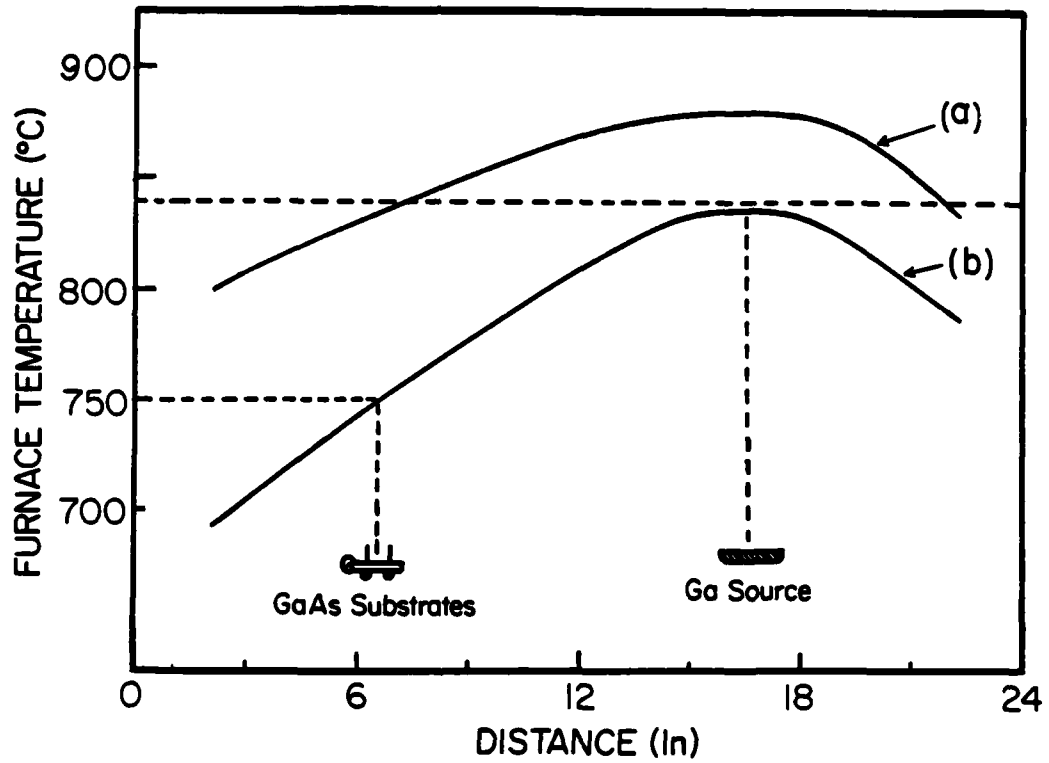


Figure 12. Temperature profile of the furnace. Curve (a) is used for the Ga-baking in H_2 and saturation with As of Ga source. Curve (b) is for the epitaxial growth

for a time to hot hydrogen bypassing the AsCl_3 bubbler. This dissolution correlates with an interfacial dip of the concentration profile.

After construction, the system was dismantled, the quartz and Pyrex parts cleaned thoroughly in aqua regia and rinsed in deionized water, the stainless steel tubing cleaned using isopropyl and trichloroethylene (one part each), and dried by nitrogen. The system has been checked for leak-tightness at each joint.

To prepare the reactor for growth the AsCl_3 (Mining and Chemical Products, 99.999% pure, in 100g ampoules) is loaded and hydrogen passed through it for several hours to distill off the first fraction. If this is not done, the first epitaxial layer will have a higher carrier concentration than normal. The final clean-up of the system to remove impurities is carried out by raising the furnace temperature to 930°C and flowing H_2 through the AsCl_3 to etch the reactor tube.

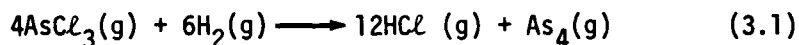
3.2 SOURCE SATURATION

The epitaxial growth of GaAs in this open tube system may be separated into two distinct processes: 1) source saturation and transport, and 2) epitaxial growth on the substrate surface. Prior to transport and epitaxial growth the Ga source must first be saturated with arsenic until a crust of GaAs forms over the liquid gallium surface. After the saturation process is complete, transport occurs from the source to the deposition region with subsequent epitaxial growth.

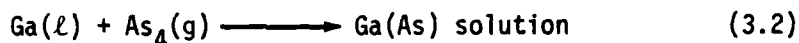
The gallium (99.99999% pure, 25 g ingots) is loaded in the source boat of the reactor. Figure 12 shows the temperature profile

of the two-zone furnace. The source temperature is about 880°C. High purity hydrogen from a palladium diffuser bypasses the AsCl_3 bubbler, whose flow rate is set to 120 ml/min. The hydrogen flow rate in the dopant line is set to 200 ml/min. After one hour Ga source baking, the valve of the bubbler is opened and hydrogen is bubbled through the AsCl_3 liquid (kept at 15°C).

During the saturation process, the hydrogen, as a carrier, transports the AsCl_3 into the reactor. The initial reaction taking place when the gas mixture heats up is



After adding the AsCl_3 into the reactor, arsenic is continuously dissolving in the gallium source



while the gallium is simultaneously removed by reaction with HCl to form volatile gallium chlorides according to the following equations:



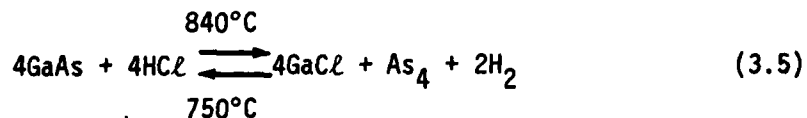
During saturation the source remains a bright homogeneous liquid. As the solution becomes saturated, a GaAs crust starts to form over the

low temperature region of the source, since the GaAs is less dense than Ga. As more arsenic is dissolved the crust extends to higher temperature regions. Finally, sufficient arsenic is dissolved to extend the crust completely over the entire source. That the source is saturated to produce a complete crust can be determined by visual observation. A completely crusted source is unstable in the absence of an AsCl_3 flow. This is due to crystallization and thickening of the crust in the low temperature region with subsequent dissolution of the crust at the higher temperature regions. Therefore, source stability is promoted by a minimum temperature gradient over the source boat.

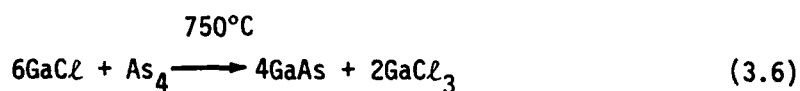
After about 8 hours of saturation under the preceding conditions, the gallium source is visually checked for saturation, the AsCl_3 and the furnace are turned off and hydrogen flow rate lowered to 60 ml/min. The system is now ready for epitaxial growth.

3.3 EPITAXIAL GROWTH PROCEDURE [29]

In the source region, the saturated source, polycrystalline gallium arsenide, is attacked by HCl around 840°C and the following reaction takes place:



At a lower temperature, in the substrate region (e.g. 750°C), solid GaAs is deposited partly by the inverse reaction, Equation (3.5), and partly by the reaction:



Since hydrogen is used as a carrier gas, the reaction of Equation (3.5) must be dominant. When the carrier gas is an inert gas (e.g. argon), the dominant equilibrium will be reaction given by Equation (3.6).

Because of differences in reactor design, residual impurities and other factors, the optimum growth conditions vary from one reactor to another. Typical growth conditions are: Ga temperature from 820° to 860°C, growth temperature from 720° to 760°C, growth temperature gradients from 5° to 15°C/cm.

The growth procedure is as follows: the furnace is turned on to the desired temperature settings first, while the reactor tubing is not in the furnace. The prepared GaAs substrate is loaded in the growth region. After the reactor tubing is properly flushed with high flow rates of hydrogen, then the hydrogen flow rates in the carrier line (with the AsCl_3 bypassed) and the dopant line are adjusted for 220 ml/min and 200 ml/min, respectively. Then the hot furnace is moved into the growth position. After about 10 minutes, the furnace temperature again approaches its steady state value, the hydrogen flow is turned through the AsCl_3 bubbler for initiation of growth. After the AsCl_3 has been turned on for 5 minutes, then the hydrogen flows in both the carrier and dopant lines are reduced to 120 ml/min and 50 ml/min, respectively.

The carrier concentration of epitaxial layer can be increased properly by adding H_2S dopants in the dopant line. After the desired growth time, the hydrogen is switched to bypass the $AsCl_3$ bubbler and the remainder of $AsCl_3$ in the reactor is purged for two minutes. Then the furnace is moved away to cool the reactor quickly. Generally, the growth rate decreases as the temperature gradient decreases. Pyramid formation during epitaxial growth is more pronounced at low growth temperature and at high $AsCl_3$ temperature and also due to the increase in the amount of Ga. On the other hand, a decrease in the density of pyramids is observed when the flow rate of H_2 is lowered. The density of these undesirable pyramids is dramatically reduced using substrates with small misorientations (2° to 5°) from (100) direction.

3.4 H_2S DOPANT INCORPORATION

The incorporation of sulfur in GaAs can be written in two steps consisting of the dissociation of H_2S and dissolution of sulfur [30]. The dissociation reaction is



The dissolution process may be written as



The overall process of doping with H_2S is the sum of reaction of Equations (3.7) and (3.8)



One of the relations between the flow rate of H_2S dopants (10 PPM in N_2) and the carrier concentration of the grown layer measured by the capacitance-voltage method is shown in Figure 13.

Sulphur does not form stable chlorides and the free sulphur equilibrium is only affected by the hydrogen and the H_2S concentration. Therefore the sulphur-doped carrier concentration is not affected by the AsCl_3 mole fraction, compared to germanium or selenium-doped crystals [31].

3.5 SUBSTRATE PREPARATION [32]

The epitaxial layers were grown on silicon doped substrates with carrier concentration $2 \times 10^{18} \text{ cm}^{-3}$. The crystallographic orientation is 2° off the (100) plane to prevent the formation of pyramids.

After the substrates are cleaved to desired dimensions, they are cleaned with organic solvents, trichloroethylene, acetone and methanol in sequence, in a beaker. The substrate is dried with bibulous paper and nitrogen. The sample is then stir-etched in a $5\text{H}_2\text{SO}_4 : 1\text{H}_2\text{O}_2 : 1\text{H}_2\text{O}$ solution for two minutes. This etchant has been mixed and cooled for ten minutes. The substrates are then rinsed in deionized water, and dried with bibulous paper and nitrogen, and loaded immediately in the reactor. The reactor is then flushed with hydrogen at high flow rates for 20 minutes before the furnace is moved to the growth position.

3.6 MATERIAL EVALUATION

The grown layer thickness is measured by the stain etching method. The sample is cleaved, etched in a mixture of

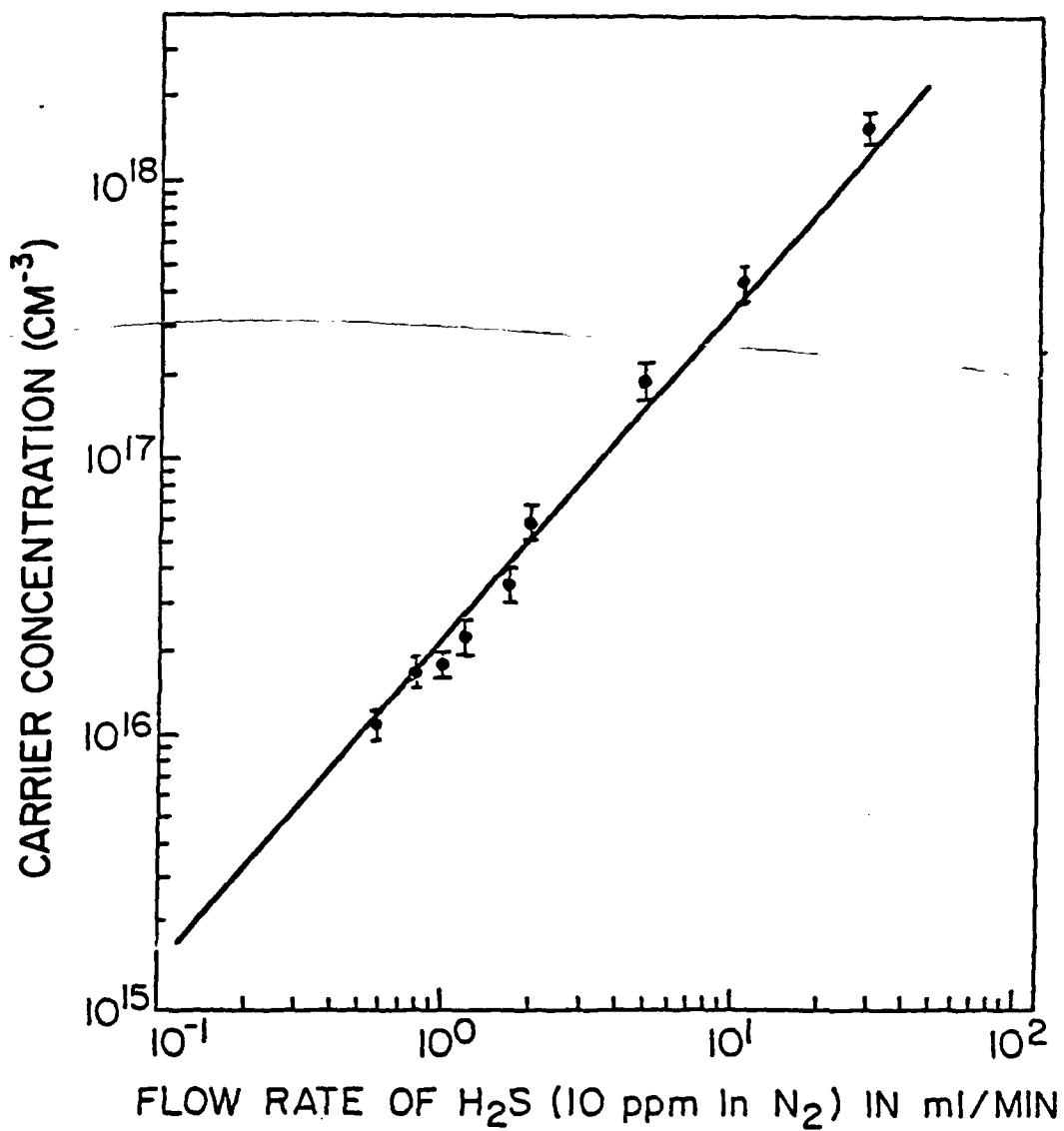


Figure 13. Doping density as a function of H₂S flow rate

1HF : 3HNO₃ : 4H₂O for about seven seconds, then viewed edgewise in a calibrated microscope. The measurement resolution is limited by how well the microscope could focus on the top rounded surface of epitaxy and interface. Depletion capacitance-voltage measurement may give a more accurate determination of epitaxial layer thickness.

The carrier concentration profiles of epitaxial layers are measured by differential capacitance technique, using 20 mil diameter dot aluminum Schottky barrier diodes. The aluminum dot is negatively biased with respect to the substrate and the capacitance of the depletion region is measured as a function of the applied bias. The doping concentration is calculated from the measured C-V data.

The effective depletion width is calculated from the measured capacitance by the simple relation

$$d = \frac{\epsilon A}{C} \quad (3.10)$$

where d = depletion depth into the epitaxy
 A = dot area
 C = depletion capacitance

The range of d over which the carrier concentration can be measured is limited by avalanche breakdown of the reverse-biased Schottky-barrier. The profiling of a layer with concentration variation can be obtained by step etching the layer to build up a piecewise profile plot.

One of the problems which often occurs in GaAs epitaxial growth is the existence of a dip in carrier concentration profile between the n layer and the n^+ substrate [33,34]. Growing a moderately doped buffer layer onto the substrate prior to the growth of the n layer can reduce the possibility of having a interfacial dip of the concentration profile.

4. DEVICE FABRICATION

In this chapter the fabrication process for Gap diode is described.

4.1 DEVICE CONSTRUCTION

The geometry of the device is a quasi-planar structure as shown in Figure 14. The n-type epitaxial layer is grown on Si doped, (100) oriented, n^+ GaAs substrate as described in Chapter 3. The thickness of the epitaxial layer is $1 \mu\text{m}$ and it has a carrier concentration of $2 \times 10^{15} \text{ cm}^{-3}$. Sulfur (H_2S) is used to dope the buffer layer. The carrier concentration profile of a representative layer is shown in Figure 15. The wafer thickness of the completed device is $80 \mu\text{m}$. The diameter of the diode is about $30 \mu\text{m}$; it can be slightly reduced by GaAs mesa etching. The widths of the ohmic contact gaps can be varied from $2.6 \mu\text{m}$ to zero. A vacuum evaporated SiO layer is used to isolate the substrate from the bonded 1 mil gold wire when the devices are packaged.

4.2 OHMIC CONTACT FABRICATION

The GaAs wafer is first mounted on a jig by using black wax with the epitaxial layer side down. The back of the sample is slowly lapped with $5 \mu\text{m}$ grit on a glass plate. The thickness of the sample is measured with a micrometer. The sample is then mounted on a glass slide using black wax to mask the epitaxial layer and then etched in a $5\text{H}_2\text{SO}_4 : 1\text{H}_2\text{O}_2 : 1\text{H}_2\text{O}$ solution. The etchant is first stirred and cooled for 10 minutes. The substrate is put in the etchant and stirred for about 10 minutes to obtain a smooth surface. The measured resultant substrate thickness is $80 \mu\text{m}$. The sample is then rinsed in deionized water and dried.

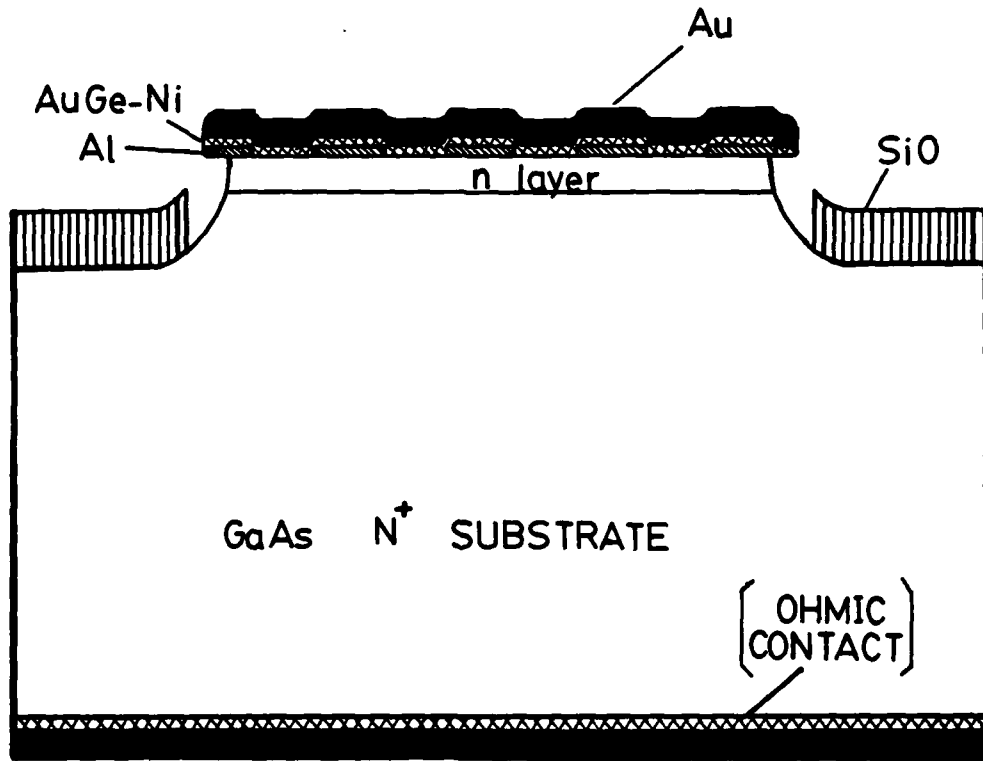


Figure 14. Cross-section of planar-type gap-controlled GaAs Schottky-barrier diode

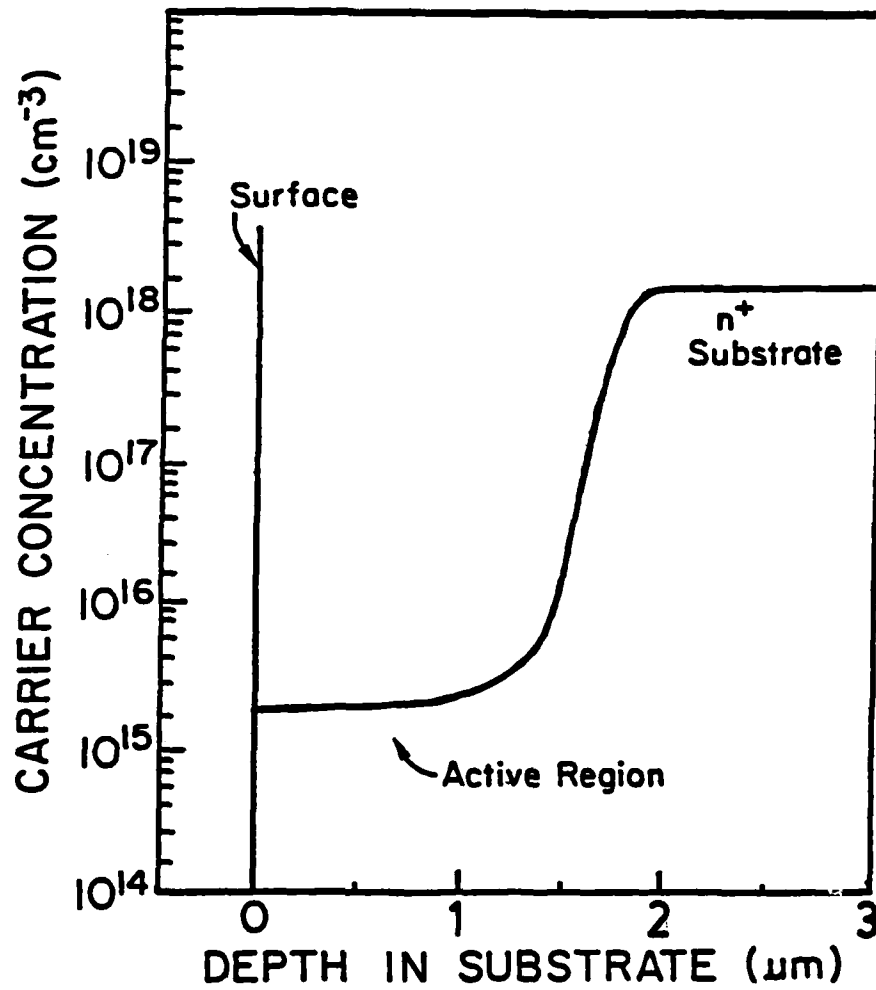


Figure 15. Carrier concentration versus depth for VPE grown layer from Schottky barrier profile measurements

After etching, the sample is loaded in a vacuum evaporator. AuGe is evaporated on the substrate side followed by a nickel evaporation. The AuGe used is eutectic composition of 88% Au, 12% Ge by weight. The thicknesses of the evaporated AuGe and Ni are monitored, the thickness ratio is about 4:1 to obtain thermally stable contacts with low contact resistance. The AuGe-Ni layer is alloyed in a furnace at 456°C for 35 seconds in a hydrogen atmosphere. The wafer is quenched by removing it quickly.

4.3 SCHOTTKY-BARRIER FABRICATION

The sample is mounted, ohmic contact side down, on a glass slide with black wax. It is then cleaned in organic solvents, trichloroethylene, acetone, and methanol, and the epitaxial layer is slightly etched in a prepared $5\text{H}_2\text{SO}_4 : 1\text{H}_2\text{O}_2 : 1\text{H}_2\text{O}$ etchant. After the sample is rinsed in deionized water and dried, it is prebaked at 120°C for 3 minutes. Then a positive photoresist, AZ1350J is spun on the sample at 10,000 RPM for 50 seconds. The photoresist is baked for 25 minutes at 75°C.

An optical mask aligner is then used to expose the photoresist. The mask contains 2.2 μm dark fringes with 1.8 μm spacings. The fringes are aligned along a cleavage plane. The exposed photoresist is developed and is then dried and postbaked for 6 minutes at 120°C. The width of the photoresist lines slightly depends on the exposure time. A photograph of the photoresist lines is shown in Figure 16. At this stage the sample appears in cross-section as in Figure 17(a). The sample is loaded in an evaporator, and 900Å thick Al is evaporated on it as shown in Figure 17(b).

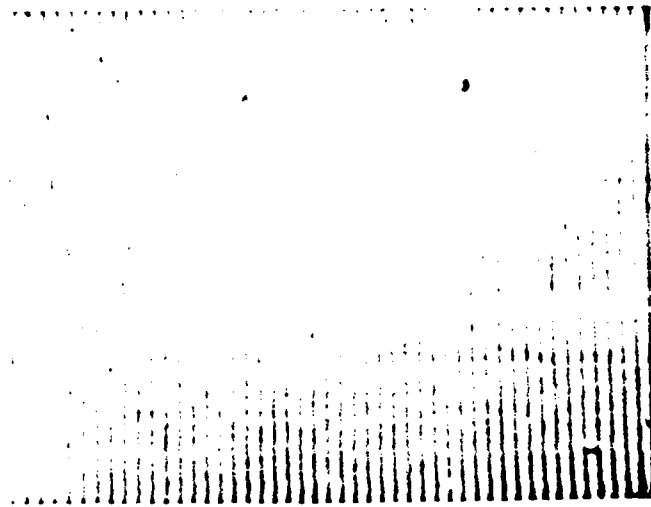


Figure 16. Photograph of 1.5 μm photoresist grating pattern on the GaAs epitaxial layer

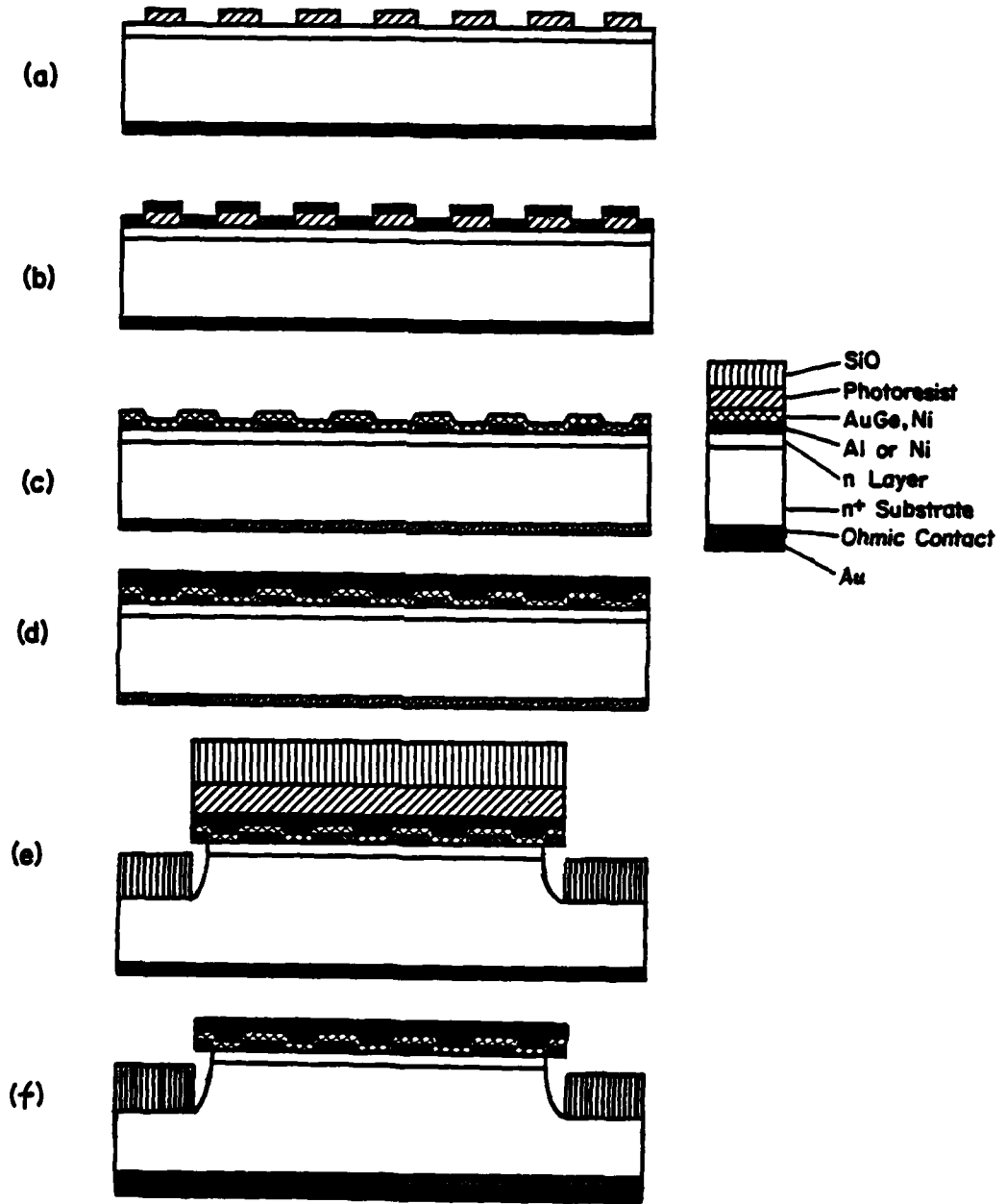


Figure 17. Process used to fabricate planar-type gap diodes

4.4 JUNCTION FORMATION

The photoresist mask is lifted by using photoresist stripper (Shipley Remover 140). After the sample is rinsed in deionized water and dried, it is loaded in the evaporator again. This time 800Å AuGe and 200 Å Ni are evaporated, respectively, on the Al lines and gaps of the sample. Then the wafer is alloyed at 456°C for 35 seconds in a hydrogen atmosphere. The preceding fabrication process is shown schematically in Figure 17(c).

The wafer is then rinsed in hydrofluoric acid for 10 seconds and rinsed in deionized water. A gold layer of about 2 μm is applied to the ohmic contact by plating the wafer in a neutral bath gold solution (Selrex Puragold 125) at 65°C. The result is shown in Figure 17(d).

After gold plating the wafer is mounted on a glass slide with substrate side down. It is cleaned in organic solvents, trichloroethylene, acetone, and methanol and prebaked again at 140°C for 15 minutes. Then filtered AZ1350J photoresist is spun on the sample at 3500 RPM for 40 seconds, and baked at 75°C for 30 minutes. The photoresist is exposed in a pattern of 32 μm diameter dot matrices. The pattern is aligned along a cleavage plane. The exposed photoresist is developed, dried and postbaked at 200°C for 40 minutes. The resultant top-view picture is shown in Figure 18.

The hardened photoresist dot is used as a mask to etch the thick Au, AuGe-Ni alloy and Al lines. The etchant is Aurostrip powder diluted in deionized water. The Aurostrip solution is heated and stirred, the wafer is immersed until all the Al and AuGe/Ni lines in between the dots are etched. The junction will be undercut more or

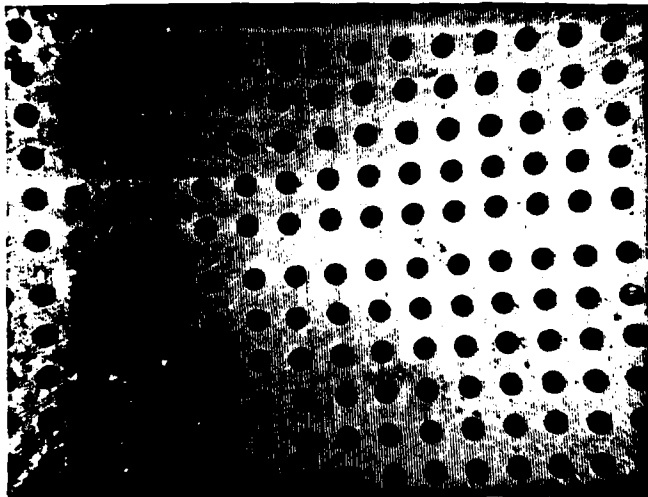
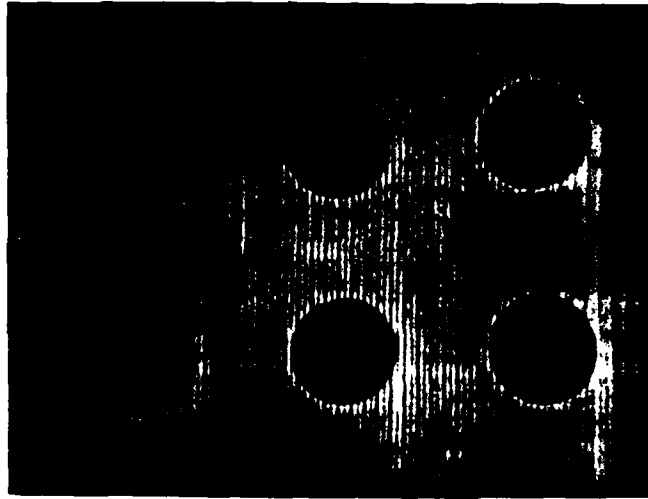


Figure 18. Photographs of 32 μm diameter. Photoresist dots on the aluminum and AuGe/Ni lines

less through the photoresist mask. One of the methods to reduce this undercutting is to make the ohmic contact and Aluminum lines thinner. Figure 19 shows unalloyed Al/AuGe/Ni dots on GaAs after metal etching.

4.5 GaAs MESA ETCH AND SiO INSULATION

After junction formation etching, the wafer with photoresist dots on it is rinsed in deionized water and baked in 120°C for 10 minutes. Then the wafer is etched in a prepared $5\text{H}_2\text{SO}_4 : 1\text{H}_2\text{O}_2 : 1\text{H}_2\text{O}$ solution to form a suitable GaAs mesa structure. At this juncture the diode area can be reduced by mesa etching the GaAs.

The wafer is rinsed in deionized water and again baked at 120°C for 10 minutes. Then it is loaded in the vacuum evaporator, and 7000 Å to 9000 Å SiO (99% pure, powder) is evaporated on the wafer, as shown in Figure 17(e). The photoresist dots are lifted by using photoresist stripper, and the fabrication is completed. Figure 20 shows photograph of several completed Gap diodes on a GaAs chip.

4.6 PACKAGING

To obtain packaged devices, the completed wafer is scribed into chips with approximately 3 x 3 diodes per chip. The chip is ultrasonically bonded in a C-2 package [35], the dimensions of the package are shown in Figure 21. Two 1 mil diameter gold wires are bonded across one diode on the chip. The photograph of the unsealed packaged diode is shown in Figure 22. Finally, the diode package is sealed with a metal lid on top of it.

In the next chapter evaluation methods and experimental results for the packaged diodes are presented.

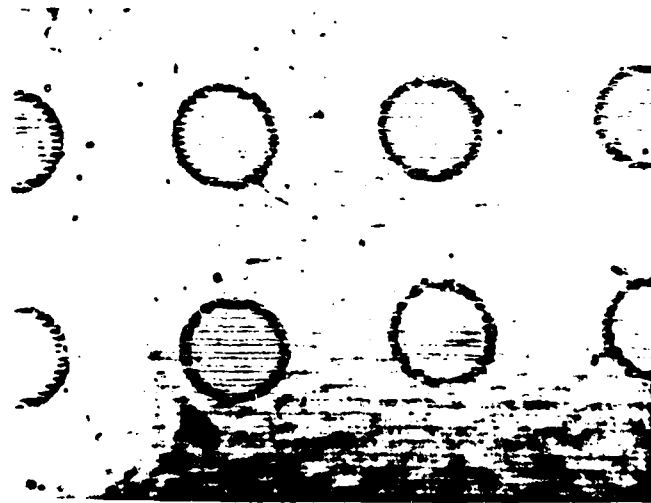


Figure 19. Photograph of unalloyed Al/AuGe/Ni stripe dots on GaAs surface after metal etching

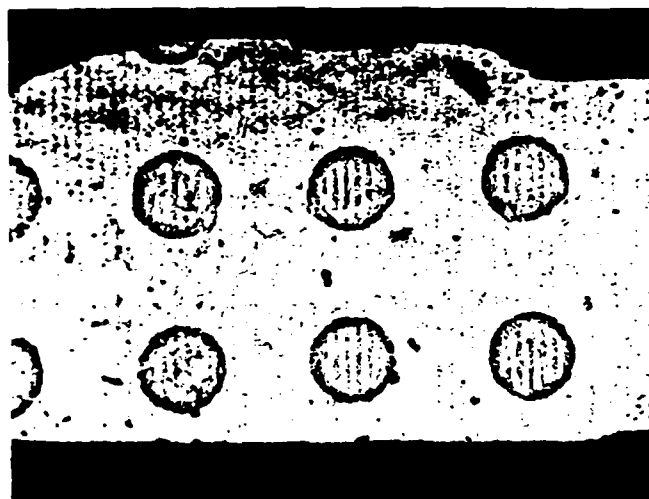


Figure 20. Completed Gap diodes on a scribed GaAs chip

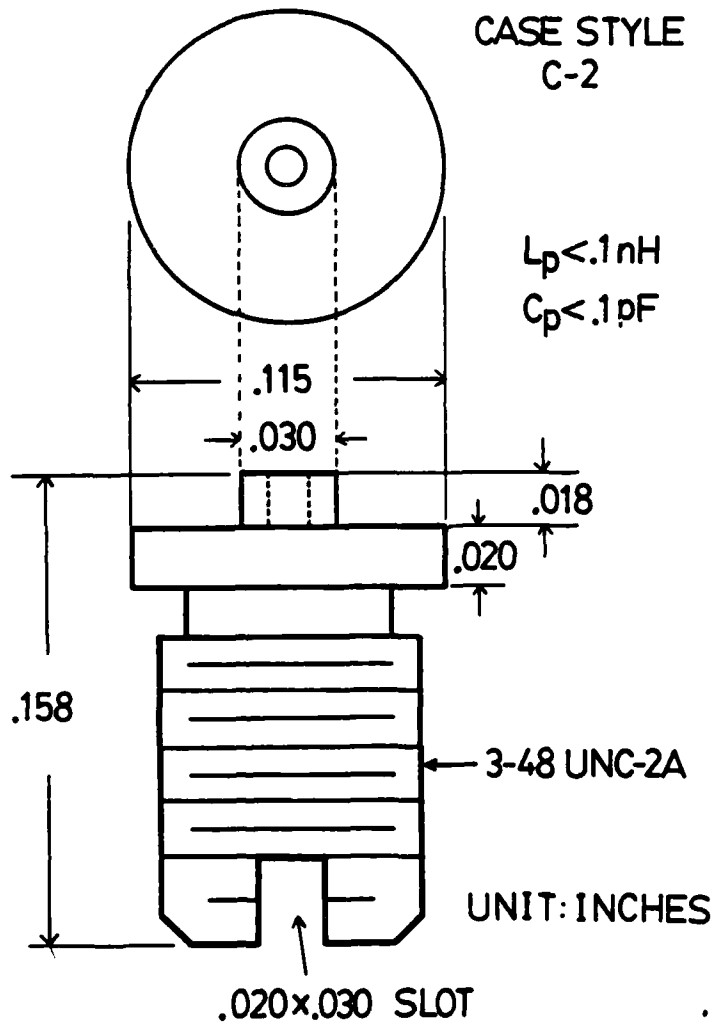


Figure 21. Dimensions of the diode package [35]



Figure 22. Photograph of a GaAs Gap diode chip mounted on a C-2 package, bonded with 1 mil Au wires

5. EXPERIMENTAL RESULTS AND DISCUSSION

In this chapter we examine the experimental behavior of the Gap diode. We will evaluate the diode current-voltage characteristics, the temperature dependence of the I-V characteristics and some of the microwave behavior of packaged devices.

5.1 CURRENT-VOLTAGE CHARACTERISTICS

Diodes were made from various thicknesses and doping concentrations of epitaxial GaAs. However, the electrical characteristics of only those diodes processed from low doped, $n=2 \times 10^{15} \text{ cm}^{-3}$, epitaxial layers will be discussed. The dimensions of the ohmic gap width are limited by the photolithography to $1 \text{ } \mu\text{m}$ to $2 \text{ } \mu\text{m}$. The zero bias depletion width from the depletion approximation, for $n=2 \times 10^{15} \text{ cm}^{-3}$, and built-in voltage $V_0=0.7 \text{ V}$, is about $0.7 \text{ } \mu\text{m}$.

Figure 23 shows various measured low-frequency I-V characteristics of the planar-type Gap diode, as the ohmic gap width, W , is gradually increased from zero to more than two depletion widths. Notice that turn-on voltages ranging from 0.7 V to nearly zero can be obtained. The diameter of these diodes is $30 \text{ } \mu\text{m}$. The right-most I-V curve in each figure is for an Al Schottky diode made by the same fabrication procedure as the Gap diodes. The reverse isolation of the planar-type Gap diode is not as good as that of the notched-type Gap diode. Hence, as the ohmic gap width opens, the reverse leakage current becomes large, as can be seen in Figure 23.

The I-V characteristics of two typical low leakage packaged planar-type Gap diodes are shown in Figure 24 on expanded scales.

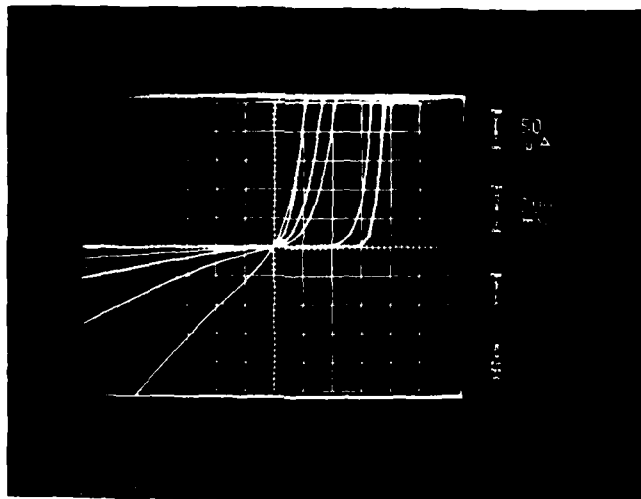
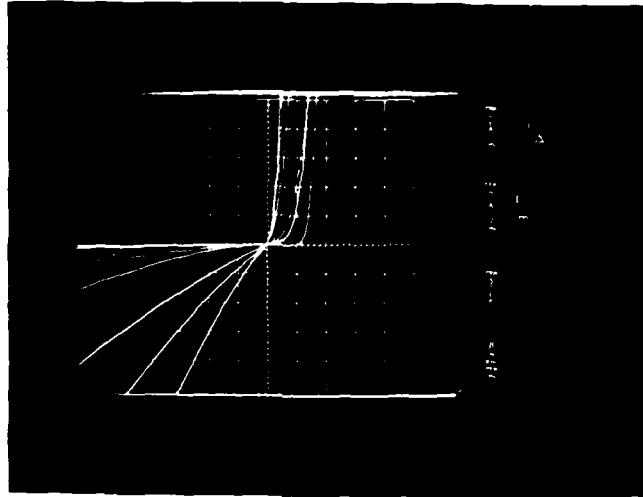


Figure 23. Photographs of various measured low-frequency I-V characteristics of the planar-type diodes as ohmic gap width, W , is gradually increased from zero to more than two depletion widths

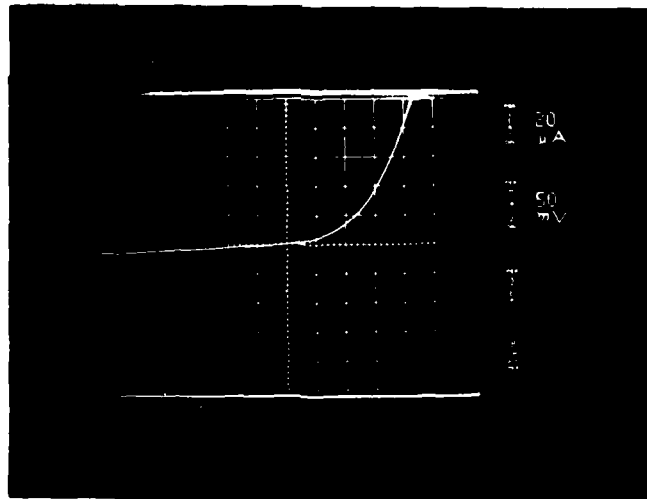
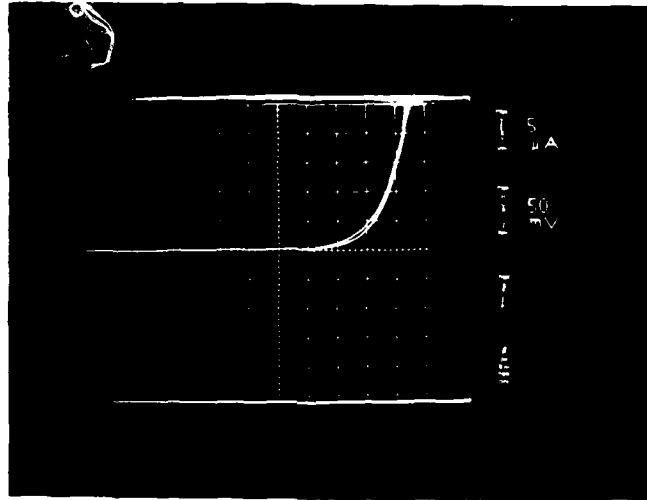


Figure 24. Photographs of I-V characteristics measured from two typical low-leakage packaged planar-type Gap diodes (Gap diode U-2, U-5)

These devices have I-V characteristics similar to those of point contact diodes, although the Gap diodes are made with very low doped epitaxial layers and large diode areas in contrast to point contact diodes.

Figure 25 shows the I-V characteristics of two wider gap-width packaged planar-type Gap diodes which show significant reverse currents. Although the turn-on voltages are low, because of the large reverse currents and corresponding low ratios of reverse resistance to forward resistance, these diodes will not yield desirable RF performance. Figure 26 and 27 show the representative I-V characteristics of two different low leakage Gap diodes on two different scales for each diode, respectively. The diode in Figure 27 has a wider ohmic gap width than that in Figure 26. These figures show that the turn-on voltage is reduced at the expense of reverse leakage current.

A detailed comparison between a Gap-diode and a pure Al Schottky diode of the same size is shown in Figure 28. The turn-on voltage of the Gap diode is lowered by 0.3 volt compared to that of the pure Schottky diode, with the reverse leakage current increased not more than one order of magnitude. The I-V relationship of the Gap diode in the forward direction still follows an exponential behavior in the low current region.

The ideality factor of the diodes calculated from the slopes in Figure 28 is about $n=1.5$. Conventional Schottky barrier devices typically have $n=1.02$. One possible explanation for this large value is that the diodes are made from low doped epitaxial layers

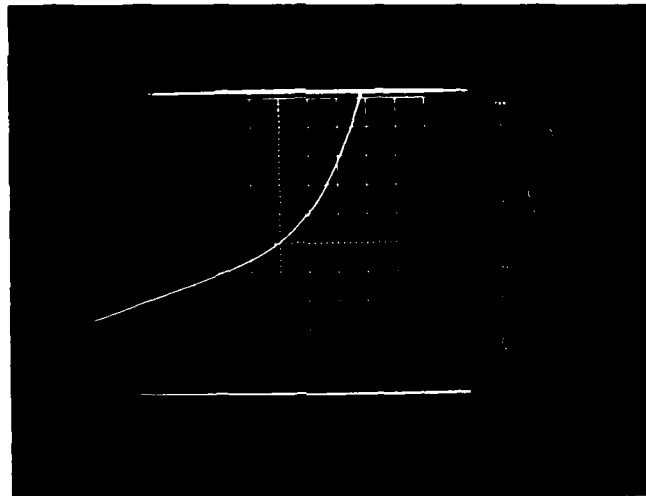
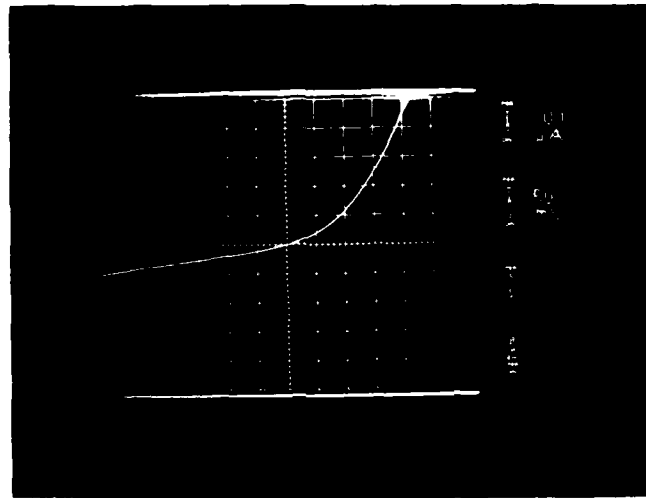


Figure 25. Photographs of I-V characteristics measured from two wide gap width packaged planar-type Gap diodes (Gap diodes T-9, E-8-B)

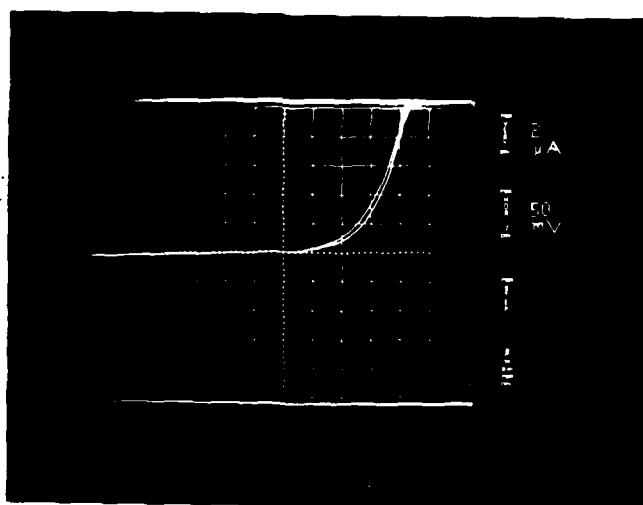
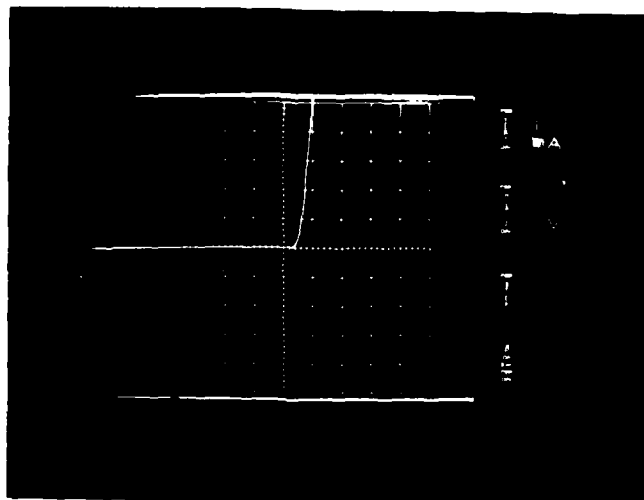


Figure 26. Photographs of I-V characteristics of a packaged planar-type Gap diode with two different current and voltage scales (Gap diode U-4)

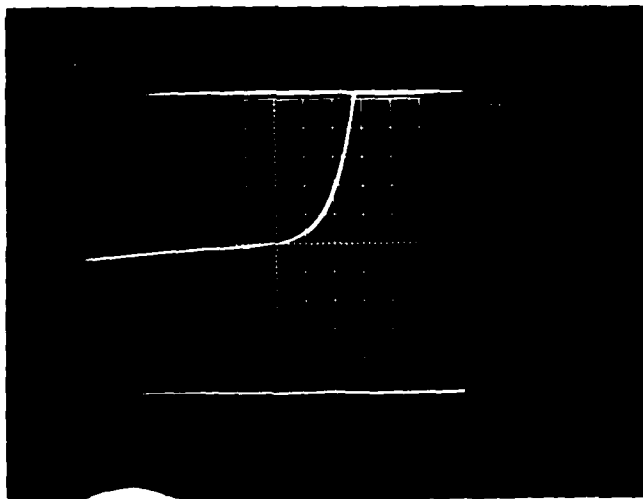
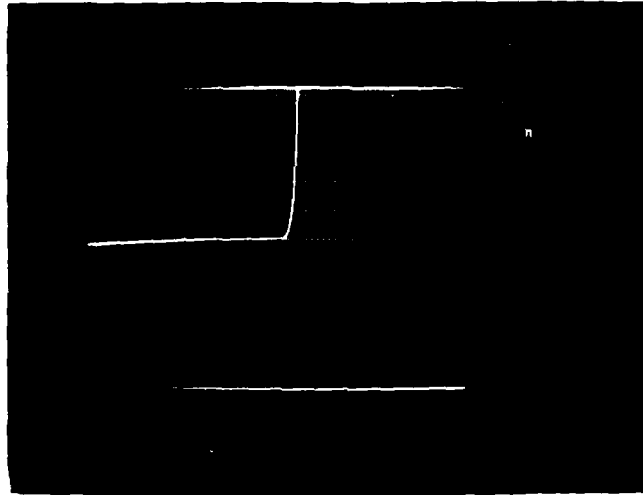


Figure 27. Photographs of I-V characteristics of a packaged planar-type Gap diode with two different current and voltage scales (Gap diode T-3)

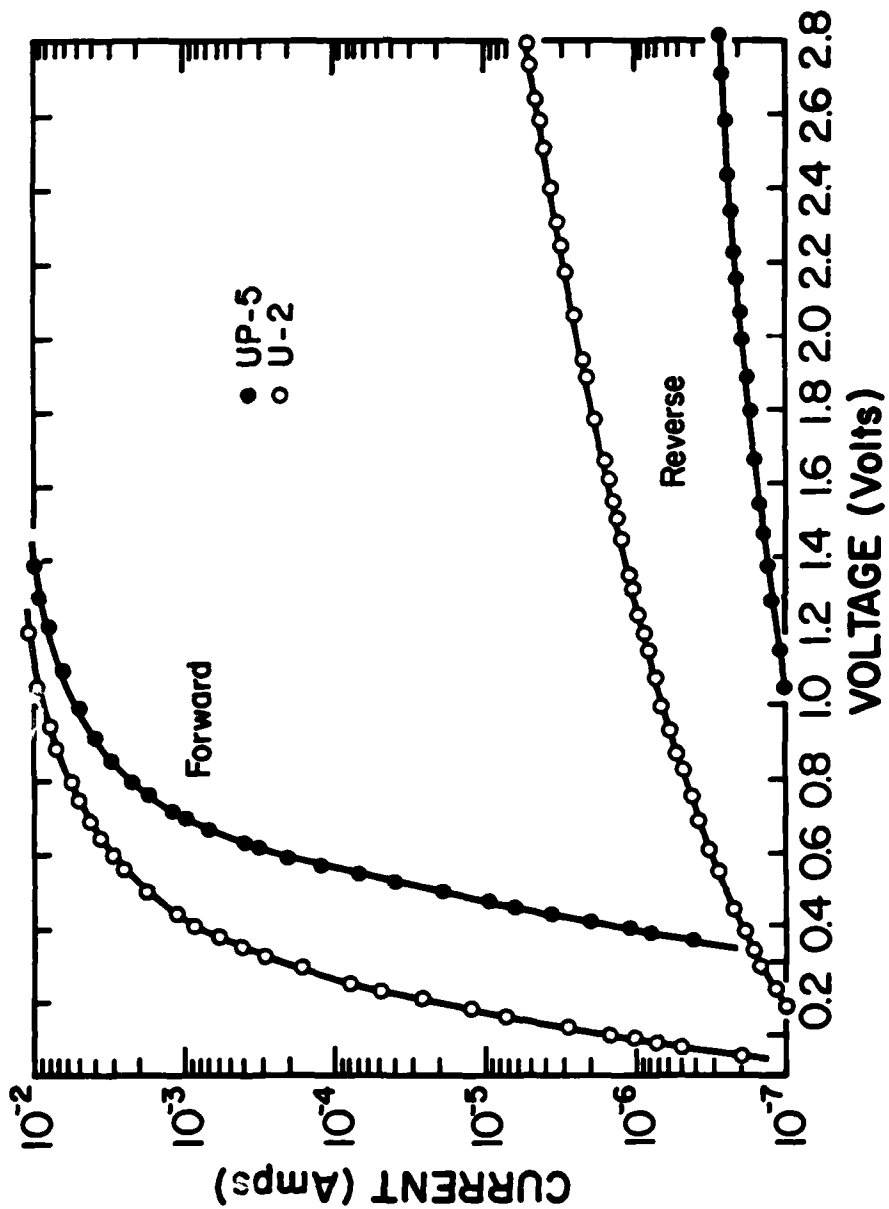


Figure 28. Representative I-V characteristics of a low-leakage Gap diode and a pure Al Schottky diode of the same size

and, therefore, the diode series resistance becomes large. Another reason may be that the Schottky-barrier junction has been alloyed at high temperature (456°C) in the fabrication procedure. High temperature anneals can degrade the properties of Schottky-barrier junctions [36].

Figure 29 compared the measured forward I-V characteristics of several Gap diodes and a pure Al Schottky diode. The differences in these I-V curves may be due to the effect of diode mesa area variations, difference in ohmic contact and Schottky contact widths, and diode packaging variations.

The Gap diode T-9, shown in Figure 29, possibly results from bonding two adjacent diodes on the chip. This would account for both the large initial slope and larger current at high voltage. At high current levels, the I-V relationship tends toward a resistance fixed by the conducting channel resistance.

Notice that in Figures 28 and 29, the currents of all the Gap diodes and the Schottky diode tend to the same value for large applied voltage. For the Gap diode, when the depleted regions are fully retracted, current is carried by the ohmic gaps and the Schottky barriers, i.e. the entire diode area is supplying current. Likewise, the entire area of the Schottky diode always supplies current. At high voltages, the effective areas of both types of devices are equal.

5.2 DIODE CAPACITANCE

The capacitance of the Gap diode is a depletion capacitance. It can be thought of in terms of two components; depletion under

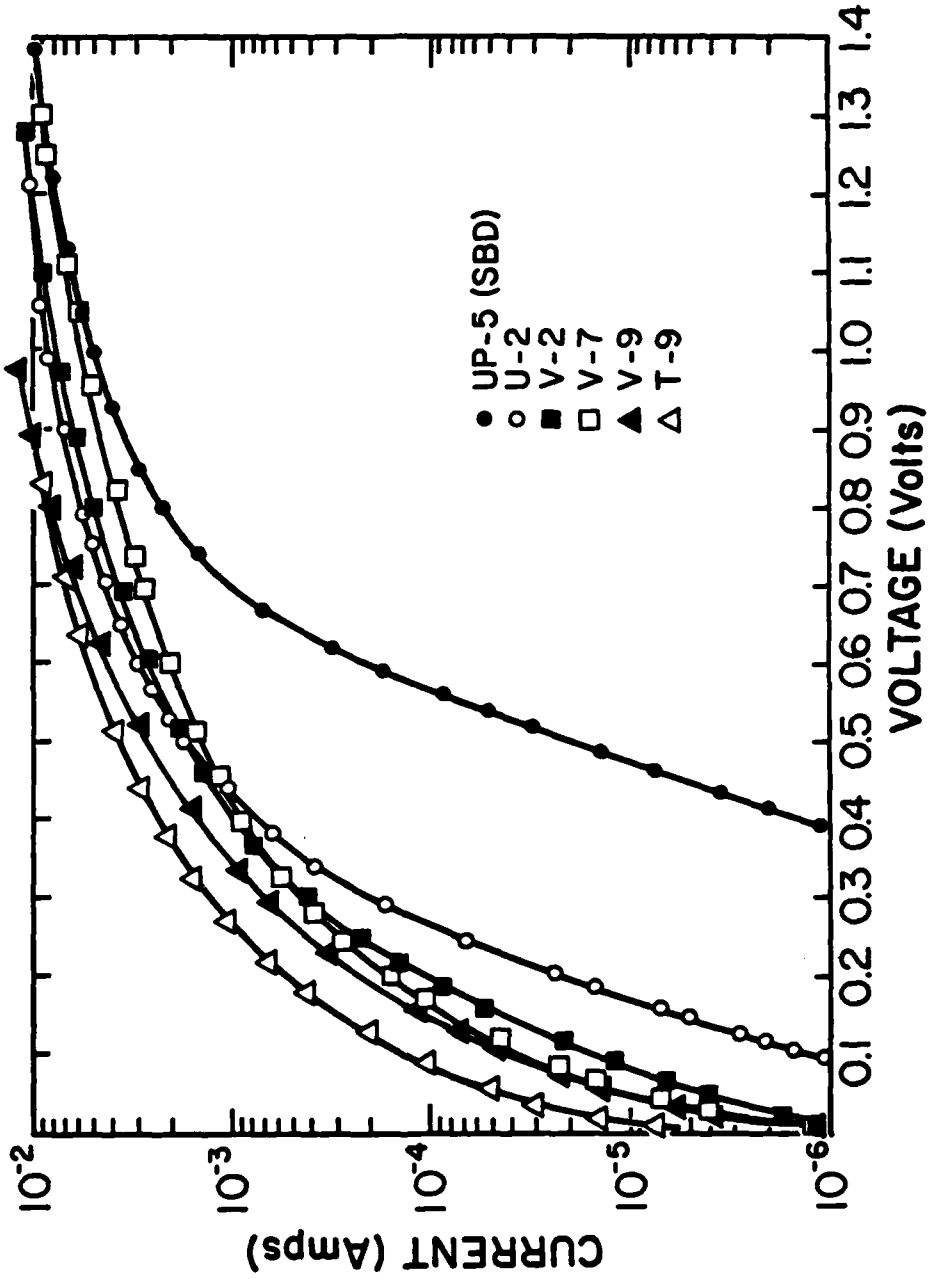


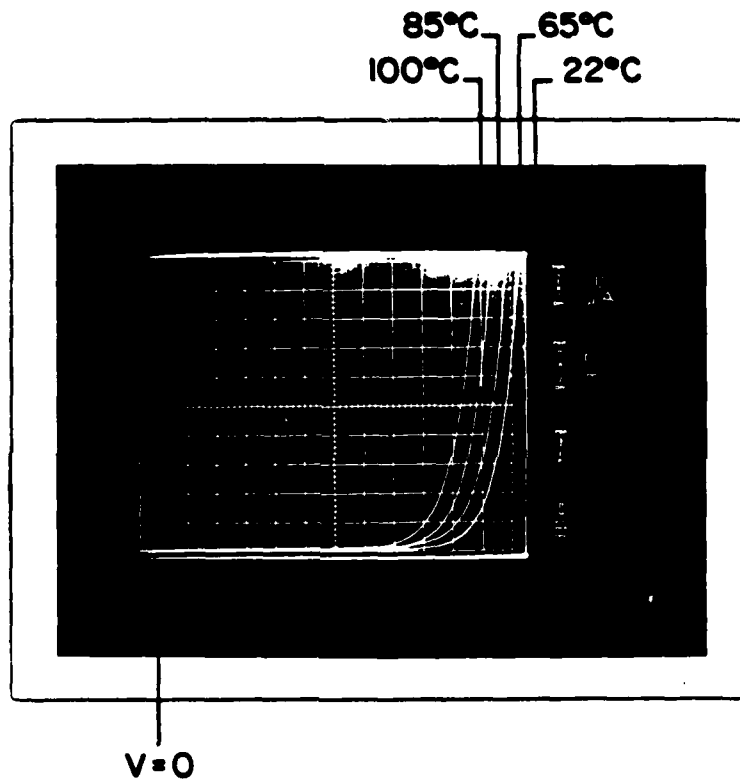
Figure 29. Measures forward I-V characteristics of several Gap diodes and a pure Al Schottky diode

the Schottky metal and that due to depletion in the gap under the ohmic metal. Preliminary capacitance measurements from packaged diodes show that, in the reverse bias direction, the capacitance decreases slightly then remains almost constant; in the forward direction, the capacitance increases rapidly beyond a bias larger than a few tenths of a volt. This is to be expected for the thin, low doped layers used. The depletion region under the Schottky contacts is punched through to the conducting substrate.

The charge distribution near the ohmic contact is complicated and a precise understanding of it is not yet well in hand. However, if one considers the model suggested in Figure 10, it can be seen that the depletion width under the ohmic contact is less than that under the Schottky metal, leading to an increased capacitance in the gap. Thus, one would expect that the zero bias capacitance of the Gap diode should increase with increased gap width until the gap is made so large that the adjacent depletion regions separate.

5.3 TEMPERATURE DEPENDENCE OF THE I-V CHARACTERISTICS

The temperature dependence of the forward I-V characteristics of a Al Schottky diode measured at four different temperatures is shown in Figure 30. The turn-on voltage of the Schottky diode is reduced by about 80 mV when the temperature is increased from 22°C to 100°C. The Schottky-barrier height is decreased as the temperature is increased, because thermionic-emission dominates in the forward bias region. However, the ideality factor decreases as temperature increases. At very low temperatures ($T < 200^\circ\text{K}$), the forward I-V characteristics tend to become independent of temperature (37). This suggests that at low



**TEMPERATURE DEPENDENCE OF SCHOTTKY BARRIER
DIODE I-V CHARACTERISTICS (V-5): $N_D = 2 \times 10^{15} \text{cm}^{-3}$,
4-WIRE BOND, Al, METALLIZATION, $D=30\mu\text{m}$**

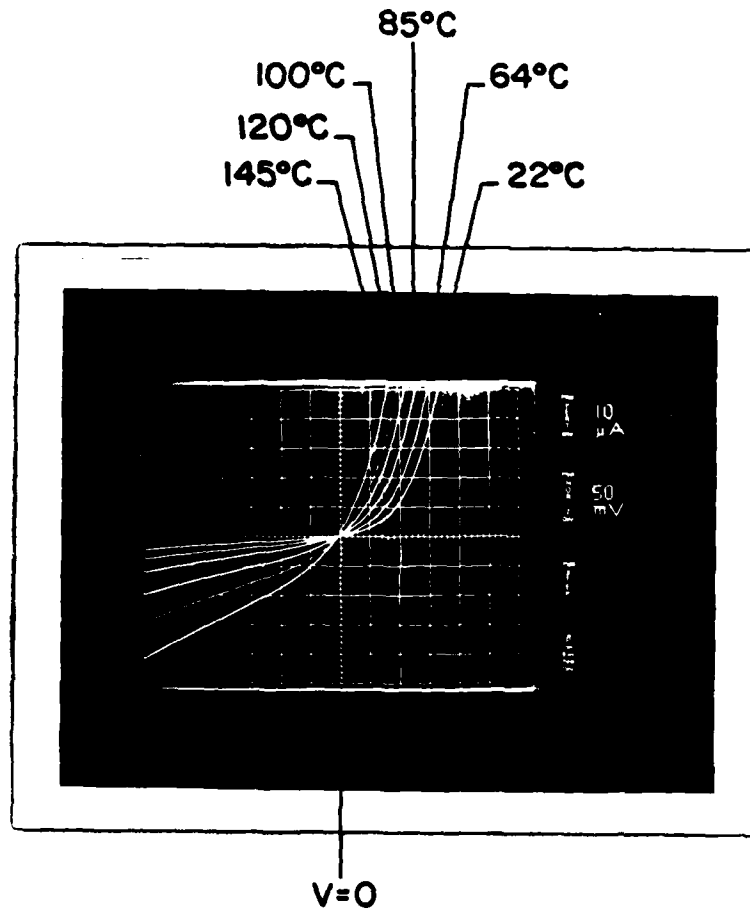
Figure 30. Photograph of the temperature dependence of the forward I-V characteristics of a Al Schottky diode measured at four different temperatures

temperatures there is a strong tendency towards quantum-mechanical tunneling.

Figure 31 shows the temperature dependence of the I-V characteristics for a Gap diode in the low current density range. It shows a positive temperature coefficient in both forward and reverse directions. The current increase due to temperature increase is larger in the forward direction than in the reverse direction. Evidently, the ohmic gap width, W , increases as the temperature increases.

Figure 32 shows the forward I-V characteristics of a pure Schottky diode and a low leakage Gap diode measured at 21°C and 100°C, respectively. The forward current of the Schottky and the Gap diode exhibits both positive and negative temperature coefficients, depending on the current density. This can be explained as follows. Under high forward bias the Gap diode and the Schottky diode are effectively identical: both devices look like resistors. Their resistance is proportional to the mobility of the n-layer which has a negative temperature coefficient.

At low bias, the Schottky diode is described by Equation 2.8 which has a positive temperature coefficient. That is, more electrons have enough thermal energy to surmount the metal-semiconductor potential barrier and so the leakage current (and the forward current) increases with temperature. There is also a secondary effect. The increased number of carriers in the undepleted material changes the equilibrium conditions; there is more diffusion, and so the depletion length is narrowed. In the Gap diode this has the effect of increasing the separation between the depleted regions under the gap thereby



TEMPERATURE DEPENDENCE OF GAP
DIODE (V2) : $N_D = 2 \times 10^{15} \text{cm}^{-3}$; 4-WIRE BOND, $D \approx 30 \mu\text{m}$

Figure 31. Photograph of the temperature dependence of I-V characteristics for a Gap diode

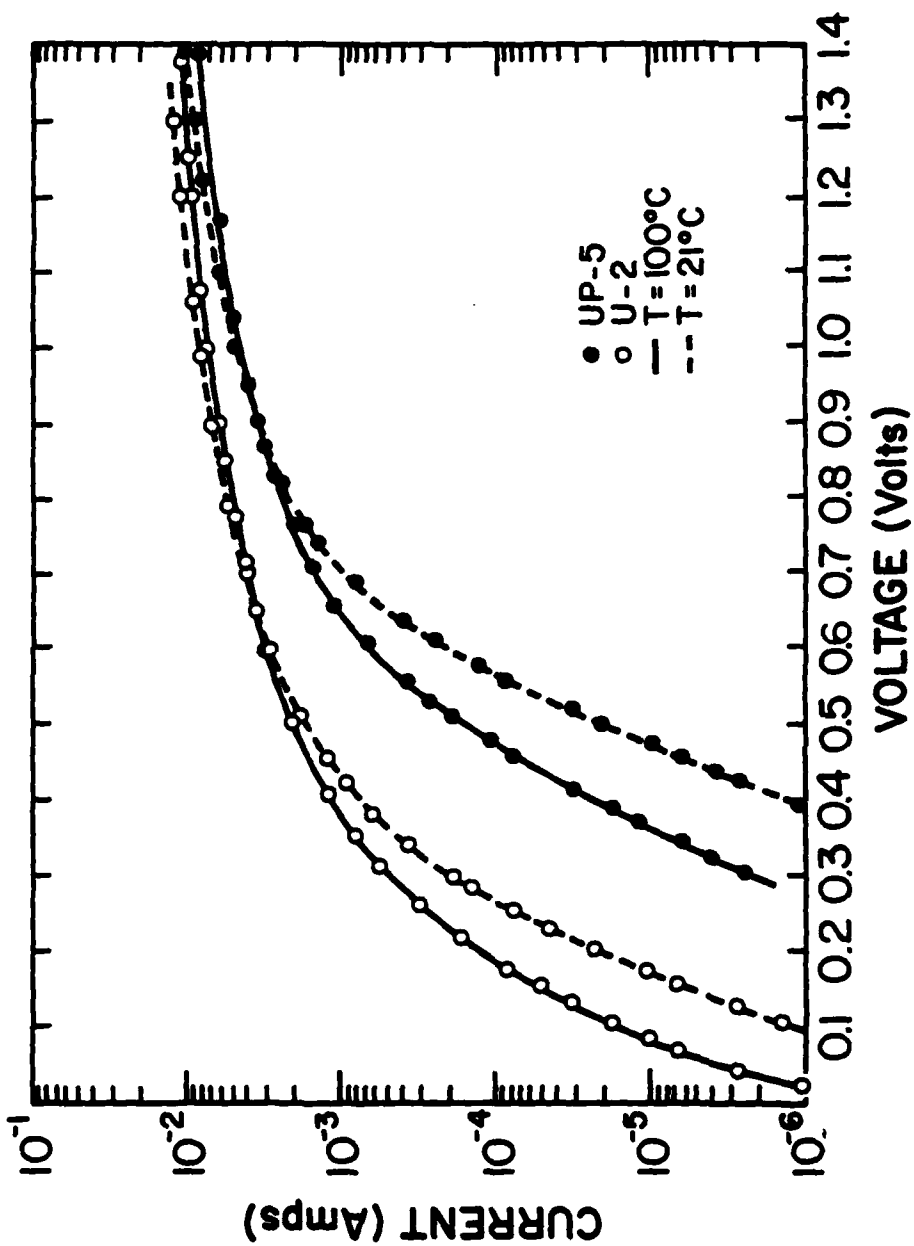


Figure 32. Forward I-V characteristics of a pure Schottky diode (UP-5) and a Gap diode (U-2) measured at 21°C and 100°C respectively

increasing the current. Presumably, the current in the Gap diode rises more slowly with temperature than in the Schottky case because the reduction in depletion width is a second order process, while the increase in current in the Schottky is proportional for T^2 and the exponential factors of Equation 2.8. This difference can be seen in Figure 32 by examining the change in current with temperature at constant (low) voltage compared to the effect of the thermally generated carriers coefficient.

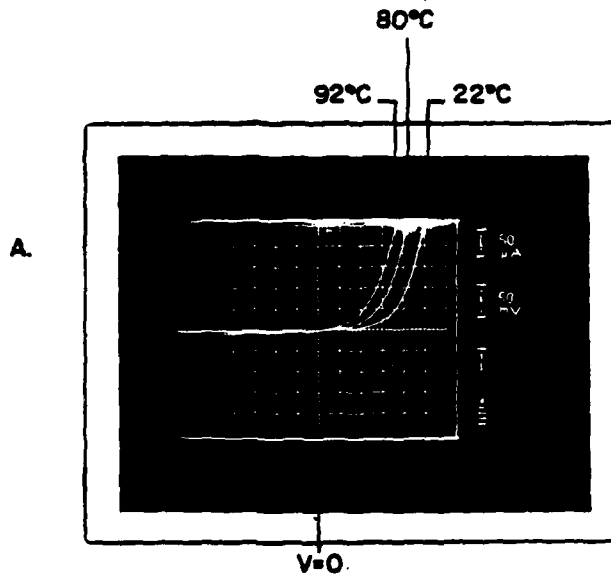
A comparison of the temperature dependence of the I-V characteristics of a Si point contact diode (1N23C) and a low leakage GaAs Gap diode is shown in Figure 33a and b. The measurements are made at three different temperatures, 22°C, 80°C and 92°C, respectively. The I-V characteristics of the Gap diode show less temperature sensitivity than those of the point contact diode. Notice that in the reverse bias direction, the point contact diode has larger leakage current.

5.4 DETECTOR CHARACTERISTICS

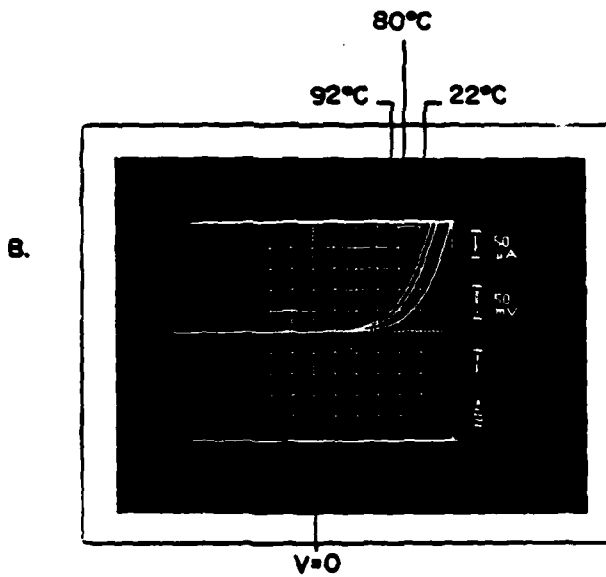
Figure 34 compares the open-circuit detected output voltage versus incident RF power of a low leakage Gap diode to those of a Si point contact diode (1N23C) and a Al Schottky diode at a frequency of 10.565 GHz. The Schottky diode is made with the same fabrication procedure as the Gap diode. All the measurements are done using the same X-band waveguide diode mount. No DC bias is applied.

The Gap diode exhibits about 3/4 the sensitivity of the 1N23C but saturates at higher power levels. When compared to a conventional Schottky diode the advantage of low turn-on voltage is readily apparent.

-78-



I-V CURVES WITH TEMPERATURE AS PARAMETER
A. IN23C: POINT CONTACT DIODE



I-V CURVES WITH TEMPERATURE AS PARAMETER
B. GAP DIODE (V-2): $N_D = 2 \times 10^{15} \text{cm}^{-3}$, 4-WIRE BOND,
 $D = 30 \mu\text{m}$

Figure 33. Photograph of temperature dependence of I-V characteristics of (a) a point contact diode (IN23C) (b) a Gap diode at 22°C, 80°C and 92°C

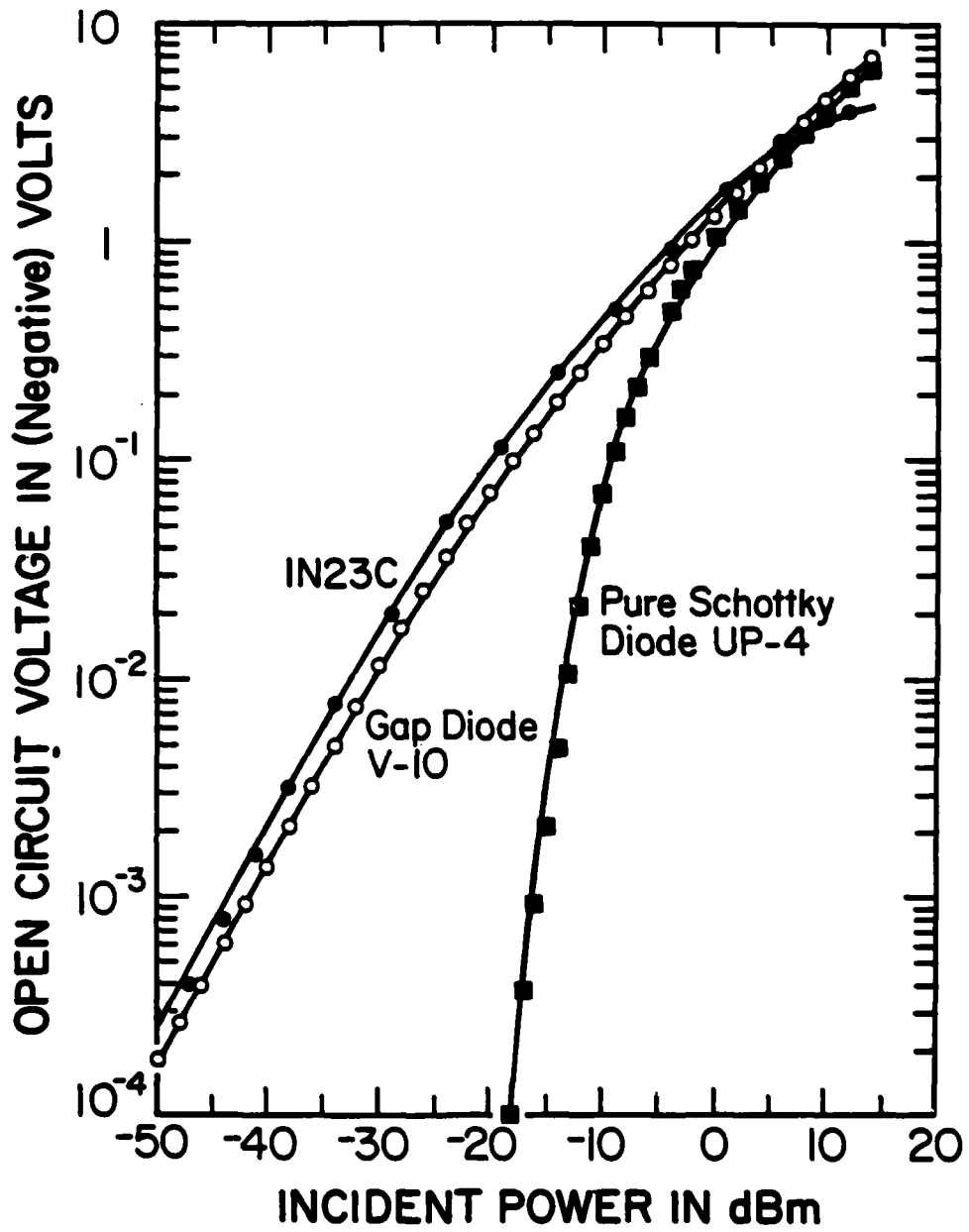


Figure 34.

Open-circuit voltage output versus incident RF power for Gap diode (V-10), point contact diode (1N23) and Schottky diode (UP-4) at 10.565 GHz

The characteristics of this device makes it a good candidate for control applications where good sensitivity and wide dynamic range are desirable.

Devices which exhibit high detectivity also have low reverse leakage current. Hence for good high frequency performance large reverse isolation, low junction capacitance and low series resistance are required. Notice that the diameter of the Gap diode used in these experiments is 30 μm , which is very large compared to that of the point contact diode, typically 2 μm . For a device design when the diode is punched-through in zero bias, the product of capacitance times voltage depends on $(N_D \mu)^{-1}$. Thus with increased carrier concentration improved performance at higher frequencies is expected.

Zero-bias detection sensitivity measurements have been carried out at several frequencies ranging from 10 to 70 GHz using the same diode in a coaxial mount, iris coupled to an input waveguide. Although these large diameter, low doped devices are far from optimum for operation at such high frequencies, surprisingly good results were obtained as seen in Figure 35.

5.5 MIXER CHARACTERISTICS

A single-ended mixer setup, as shown in Figure 36, was used to measure the conversion loss of the Gap diode. The IF impedance transformer was chosen to provide a 50 Ω to 400 Ω transformation. The adjustable matching network is an LC π circuit. The best device showed conversion loss of 6.1 dB at 10.5 GHz, including 1 dB insertion loss in the 20 MHz IF impedance matching network. The lowest conversion loss observed for the 1N23C point contact diode in the same mount is 9 dB.

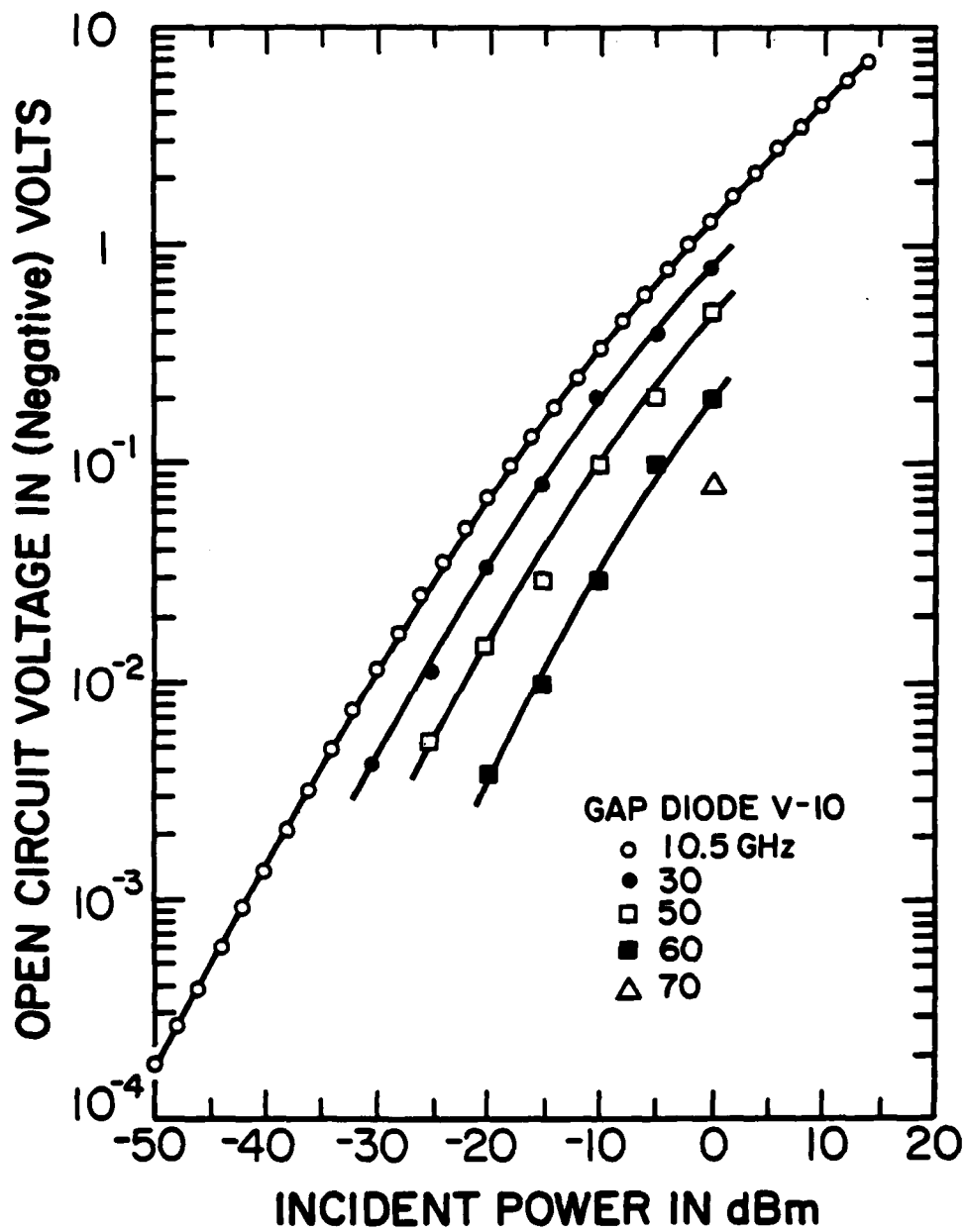


Figure 35. Open-circuit voltage output versus incident RF power of a Gap diode (V-10)

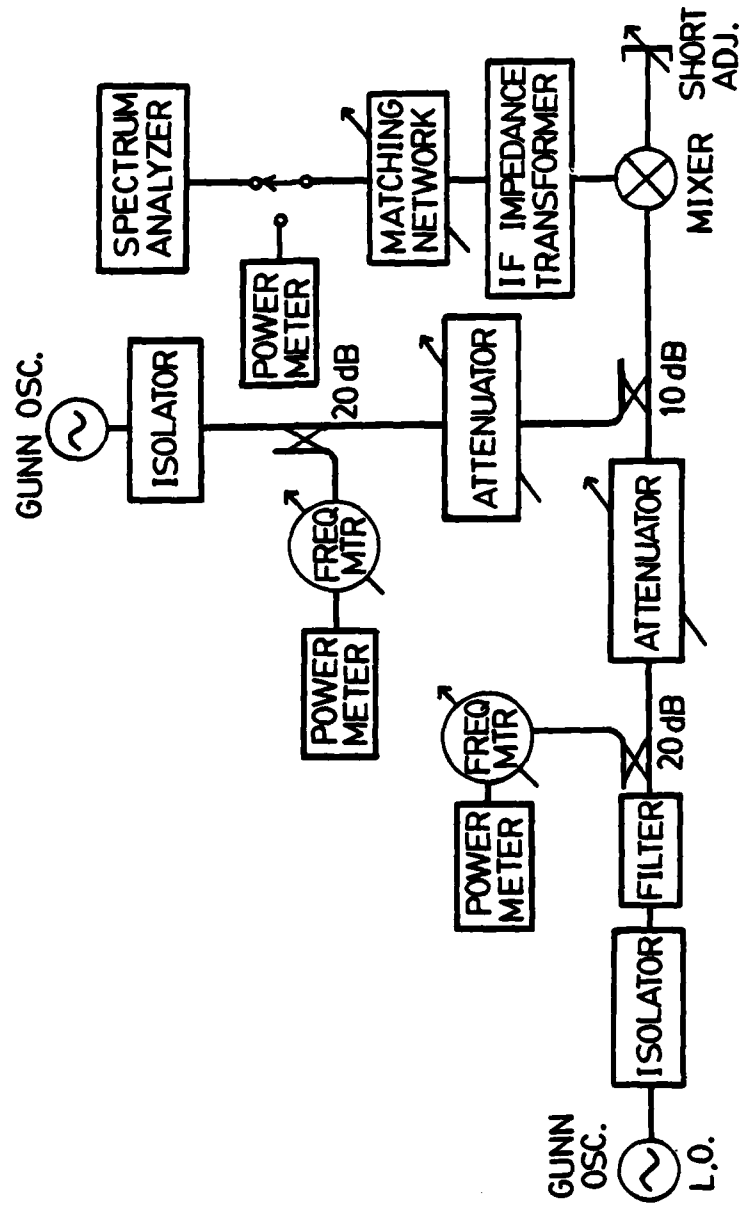


Figure 36. Single-ended mixer conversion loss measuring setup

Figure 37 shows conversion loss versus local oscillator power for three Gap diodes with different ohmic gap widths at 20 MHz IF and 10.5 GHz RF. Gap diode U-3 has the smallest gap. Its conversion loss is the lowest under high local oscillator drive conditions. As the local oscillator power is decreased the conversion loss increases rapidly, similar to the behavior of a conventional Schottky diode.

In Figure 37, the gap width of the diodes shown increases from right to left. The conversion loss of diode U-7 in the high local oscillator power region is larger than that of the other two diodes, because of its larger reverse leakage. On the other hand, diode U-7 shows lower conversion loss at low local oscillator powers, owing to its lower turn-on voltage. The measured conversion loss versus local oscillator power relationship for the 1N23C point contact diode is similar to that of Gap diode U-7. Consequently, the best Gap diode for detector and mixer applications will be that with low turn-on voltage and good reverse isolation.

The principal factors limiting diode performance are the junction capacitance C_j and series resistance R_s . Junction capacitance C_j allows current to bypass the nonlinear diode resistance R_j while series resistance R_s is a source of power dissipation, heat generation and excess diode noise. The diode conversion loss is directly proportional to the product of diode junction capacitance and series resistance. Therefore, better conversion efficiency and noise performance are to be expected if the device carrier concentration is made higher and the ohmic gap width and diode dimensions reduced.

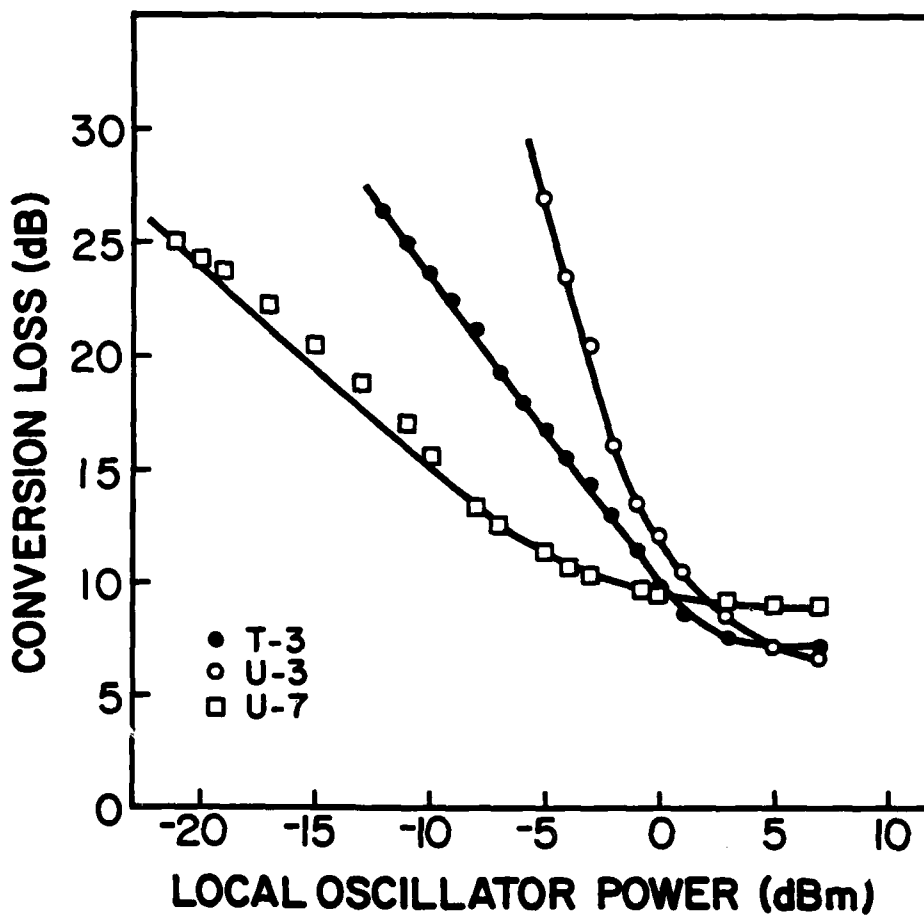


Figure 37. Single-ended mixer conversion loss versus local oscillator power for three different Gap diodes (at 10 GHz RF, 20 MHz IF). The ohmic gap width increases from diode U-3 to diode U-7

6. CONCLUSIONS

A survey has been made of the techniques which may be used to control and vary the effective barrier height of metal-semiconductor diodes. The physical properties of Schottky-barrier and ohmic contacts have been discussed. A new low turn-on voltage gap-controlled Schottky diode and simple design theories for it have been presented.

Experimental results show the turn-on voltage of the Gap diode can be controlled by varying the width of the ohmic gap. Some of the I-V characteristics and detector sensitivities of the Gap diode are similar to those of Si point contact diodes. Preliminary results show the Gap diode to be less temperature sensitive than the point contact diode. The burn-out properties of the Gap diode are expected to be better than those of the pure Schottky diode, and its noise properties also may be significantly different. The noise and the burn-out behavior of the Gap diode need investigation.

Preliminary RF characteristic measurements show considerable promise for the Gap diode. Its cutoff frequency can be increased by reducing the ohmic gap width and the diode area, and by increasing the epitaxial doping concentration. Optimum Gap diode configurations for very high frequency applications need to be explored, especially when high field transport in submicron devices is considered. Better photolithographic technology is needed for the fabrication of smaller ohmic gap widths. Other shapes of gap openings, in addition to the two presented in this report, may be considered.

The depletion approximation picture of the Gap diode, as discussed in Chapter 2, is not sophisticated enough to accurately predict all aspects of device performance. This is because detailed knowledge of the free carrier distribution near the contact is not included in the model. However, even such a crude representation is helpful in understanding the influence of the geometric and material parameters on device behavior. For example, the calculated results from the analytic I-V relationship for notched-type diodes, shown in Figure 7, have similar shapes to the experimental results obtained for planar-type diodes. See Figure 29.

The I-V curves in Figure 7 are calculated using the condition that the channel is not pinched off. That is, the zero bias depletion regions in the gap do not touch. As the ohmic gap width W is increased, the I-V relation deviates from the narrow gap exponential behavior to a more linear (resistive) one. This prediction agrees well with that observed experimentally as can be seen for the wide gap diode of Figure 29, labeled V-9. Notice, also, that the currents for large forward voltage (10mA at $V=1V$) are well predicted by theory.

For the case of narrow gap devices, such as that represented by diode U-2 of Figure 29, the analytical model fails since it predicts zero current when the gap region is pinched off. In the physical device, this is not the case since there will be a significant number of free carriers within a few Debye lengths of the edge of the heavily depleted region [38] which contribute to the current. Likewise, the effect of the ohmic contact on carrier distribution in the gap is not known in detail. It is likely that the ohmic contact is not truly

that, but rather a low barrier Schottky one. The influence of the low barrier height will not be significant for wide gap devices where the depleted regions separate with the application of a small forward bias. However for narrow gap ones, since the potential drop laterally (across the gap) will be small, the depletion regions will not retract at the same rate as when the free channel is exposed, and so, the influence of a low barrier contact may be magnified in this case. For very small gaps the behavior is dominated by the Schottky contacts and the I-V curve approaches that for a pure Schottky diode.

The electrical performance of a diode is controlled by its I-V characteristics. Since the Gap diode I-V relationship is not necessarily exponential one might anticipate that non-linear effects such as intermodulation distortion, harmonic generation, etc., may be controlled by adjusting the shape of the I-V curve. For designing an optimum diode configuration with low turn-on voltage, low reverse leakage, and high cut-off frequency an efficient numerical analysis will be required [39].

We have demonstrated a new device principle. It is possible to produce depletion of carriers under ohmic contact regions. This observation can be applied to other two and three terminal structures which may yield microwave and millimeter wave devices with new and desirable properties.

With the techniques discussed above, the effective barrier height of metal-semiconductor contacts can be varied and controlled in the range below the true barrier height. Therefore, it also may be used as a tool or design approach for other device applications.

7. ACKNOWLEDGEMENT

The authors wish to thank James E. Holtz and Bobby G. Atkinson of the Central Microwave Company, St. Charles, Missouri, for helpful discussions on device processing and assistance in device packaging.

AD-A116 162 WASHINGTON UNIV SEATTLE DEPT OF ELECTRICAL ENGINEERING F/6 20/12
CONTROL OF GAAS MICROWAVE SCHOTTKY DIODE ELECTRICAL CHARACTERIS--ETC(U)
MAY 82 S J TENG, R E GOLDWASSER N00014-79-C-0840
UNCLASSIFIED TR-ONR-82-1 NL

2 1 2

01

01

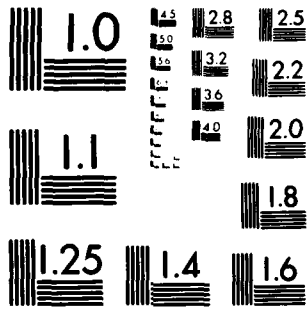
01

END

DATE

7 82

DTIC



MICROCOPY RESOLUTION TEST CHART
NATIONAL BUREAU OF STANDARDS 1963-A

8. BIBLIOGRAPHY

- [1] A.M. Cowley, H.O. Sorensen, "Quantitative Comparison of Solid-State Microwave Detectors", IEEE Transactions on Microwave Theory and Techniques, Vol. MTT-14, No. 12, pp. 588-602, December 1966.
- [2] Y. Anand, W.J. Moroney, "Microwave Mixer and Detector Diodes", Proceedings of the IEEE, Vol. 59, No. 8, pp. 1182-1190, August 1971.
- [3] C.F. Genzabella, C.M. Howell, "Gallium Arsenide Schottky Mixer Diodes", Institute of Physics Conference Series Number 3, pp. 131-137 (1967).
- [4] S.M. Sze, "Physics of Semiconductor Devices", Wiley, New York (1969).
- [5] E.H. Rhoderick, "The Physics of Schottky Barriers", Oxford University Press, Oxford (1978).
- [6] J. Bardeen, "Surface States and Rectification at Metal Semi-Conductor Contact", Physics Review, 71, pp. 717-727, (1947).
- [7] C.A. Mead, "Ohmic Contacts to Semiconductors", Electrochemical Society (Edited by B. Schwartz), pp. 3-16, (1969).
- [8] R.A. Scranton, J.S. Best, J.O. McCaldin, "Highly Electronegative Contacts to Compound Semiconductors", Journal of Vacuum Science and Technology, 14(4), 930 (1977).

- [9] J.M. Shannon, "Control of Schottky Barrier Height Using Highly Doped Surface Layers", Solid-State Electronics, Vol. 19, pp. 537-543, (1976).
- [10] V.L. Rideout, "A Review of the Theory and Technology for Ohmic Contacts to Group III-V Compound Semiconductors", Solid-State Electronics, Vol. 18, pp. 541-550, (1975).
- [11] W.J. Moroney, Y. Anand, "Low Barrier Height GaAs Microwave Schottky Diode Using Gold-Germanium Alloy", 1970 Symposium on GaAs, Paper 31, pp. 259-267 (1970).
- [12] C.J. Madams, D.V. Morgan, J.M. Howes, "Outmigration of Gallium from Au-GaAs Interfaces", Electronic Letters, Vol. 11(24), 574 (1975).
- [13] G. Dearnaley, H. Freeman, S. Nelson, J. Stephen, Ion Implantation. North Holland, Amsterdam (1974).
- [14] J.M. Shannon, "Reducing the Effective Height of a Schottky Barrier Using Low Energy Ion Implantation", Applied Physics Letters, 24(8), 369 (1974).
- [15] P.D. Taylor, D.V. Morgan, "The Effects of Radiation Damage on the Properties of Ni-nGaAs Schottky Diodes - II", Solid-State Electronics, 19, 481 (1976).
- [16] W.E. Dahlke, S.M. Sze, "Tunneling in Metal-Oxide-Silicon Structures," Solid-State Electronics, 10, 865 (1967).

- [17] A.S. Ashok, J.M. Borrego, R.J. Gutmann, "A Note on the Evaluation of Schottky Diode Parameters in the Presence of an Interfacial Layer", Electronics Letters, Vol. 14, 332 (1978).
- [18] B.R. Pruniaux, A.C. Adams, "Dependance of Barrier Height of Metal-Semiconductor Contact (Au-GaAs) on Thickness of Semiconductor Surface Layer", Journal of Applied Physics, 43(4), 1980 (1972).
- [19] C.H. Wei, S.S. Yee, "Comments on Dependence of Barrier Height of Metal-Semiconductor Contact (Au-GaAs) on Thickness of Semiconductor Surface Layer", Journal of Applied Physics, 45(2) 971 (1974).
- [20] W. Schottky, *Naturwissenschaften* 26, 843 (1938).
- [21] C.R. Crowell, "The Richardson Constant for Thermionic Emission in Schottky Barrier Diodes", Solid-State Electronics, Vol. 8, pp. 395-399 (1965).
- [22] V.L. Rideout, C.R. Crowell, "Effects of Image Force and Tunneling on Current Transport in Metal-Semiconductor (Schottky Barrier) Contacts", Solid-State Electronics, Vol. 13, pp. 993-1009 (1970).
- [23] S.M. Sze, C.R. Crowell, D. Kahng, "Photoelectric Determination of the Image Force Dielectric Constant for Hot Electrons in Schottky Barriers", Journal of Applied Physics, Vol. 35, No. 8, pp. 2534-2536 (1964).

- [24] M.N. Yoder, "Ohmic Contacts in GaAs", Solid-State Electronics, Vol. 23, pp. 117-119 (1979).
- [25] M. Wittmer, T. Finstad, M.A. Micolet, "Investigation of the Au-Ge-Ni and Au-Ge-Pt System Used for Alloyed Contacts to GaAs", Journal of Vacuum Science and Technology, Vol. 14, No. 4, 935 (1977).
- [26] G.Y. Robinson, "Metallurgical and Electrical Properties of Alloyed Ni/Au-Ge Films on N-Type GaAs", Solid-State Electronics, Vol. 18, pp. 331-342 (1975).
- [27] Y. Mochida, J.I. Nishizawa, T. Ohmi, R.K. Gupta, "Characteristics of Static Induction Transistor: Effects of Series Resistance", IEEE Transactions on Electron Devices, Vol. ED-25, pp. 761-767, July 1978.
- [28] J.R. Knight, D. Effer, P.R. Evens, "The Preparation of High Purity Gallium Arsenide by Vapor Phase Epitaxial Growth", Solid-State Electronics, Vol. 8, pp. 178-180 (1965).
- [29] L. Hollan, J.M. Durand, R. Cadoret, "Influence of the Growth Parameters in GaAs Vapor Phase Epitaxy", Journal of the Electrochemical Society, Vol. 124, No. 1, pp. 135-139, January 1977.
- [30] P. Pai-Choudhury, "Thermodynamics of Ga-AsCl₃-H₂ System and Dopant Incorporation", Journal of Crystal Growth 11, 113 (1971).

- [31] J.V. DiLorenzo, G.E. Moore, Jr., "Effects of the $AsCl_3$ Mole Fraction on the Incorporation of Germanium, Silicon, Selenium, and Sulfur into Vapor Phase Epitaxial Layers of GaAs", Journal of the Electrochemical Society, Vol. 118, No. 11, November 1971.
- [32] M. Otsubo, T. Oda, S. Mitsui, H. Miki, "The Effect of Substrate Preparations on the Surface Morphologies of the Epitaxial Layers of GaAs", Journal of the Electrochemical Society, Vol. 124, No. 12, pp. 1907-1912, December 1977.
- [33] F. Hasegawa, T. Saito, "Occurrence of a High Resistance Layer at Vapor Epitaxial GaAs Film-Substrate Interface", Japanese Journal of Applied Physics, 7, 1125 (1968).
- [34] H. Sato, S. Iida, "A Thin GaAs N on N^+ Epitaxial Film with Abrupt Interface in Carrier Concentration Profile", Japanese Journal of Applied Physics, 9, 156 (1970).
- [35] Diode Package, Central Microwave Company, St. Charles, Missouri 63301.
- [36] H.J. Hovel, C. Lanza, "The Behavior of Schottky Barriers to GaAs as a Function of Annealing Temperature", IEEE Transactions on Electron Devices, Vol. ED-27, No. 11, November 1980.
- [37] R. Hackam, P. Harrop, "Electrical Properties of Nickel-Low-Doped n-type Gallium Arsenide Schottky-Barrier Diodes", IEEE Transactions on Electron Devices, Vol. ED-19, pp. 1231-1238, December 1972.

- [38] K. Yamaguchi, H. Kadera, "Drain Conductance of Junction Gate FET's in the Hot Electron Range," IEEE Transactions on Electron Devices, Vol. ED-23, pp. 545-553, June 1976.
- [39] P. Chen, "Numerical Analysis of Semiconductor Devices Using Small Computers," Washington University, St. Louis, D.Sc. Dissertation, 1982.

DISTRIBUTION LIST - SPECIAL REPORT
 CONTRACT NO0014-79-C-0840

1/81

Code 427 Office of Naval Research Arlington, VA 22217	4	Dr. H. C. Nathanson Westinghouse Research and Development Center Beulah Road Pittsburgh, PA 15235	1
Naval Research Laboratory 4555 Overlook Avenue, S. W. Washington, D. C. 20375 Code 6811 6580	1 1	Dr. F. Eisen Rockwell International Microelectronics Center P. O. Box 1085 Thousand Oaks, CA 91360	1
Defense Documentation Center Building 5, Cameron Station Alexandria, VA 22314	12	Dr. C. Krumm Hughes Research Laboratory 3011 Malibu Canyon Road Malibu, CA 90265	1
Dr. Y. S. Park AFWAL/DHR Building 450 Wright-Patterson AFB Ohio, 45433	1	Mr. Lothar Wandinger ECOM/AMSEL/TL/IJ Fort Monmouth, NJ 07003	1
ERADCOM DELET-M Fort Monmouth, NJ 07703	1	Dr. Harry Wieder Naval Ocean Systems Center Code 922 271 Catalina Blvd. San Diego, CA 92152	1
Texas Instruments Central Research Lab M.S. 134 13500 North Central Expressway Dallas, TX 75265 Attn: Dr. W. Wisseman	1	Dr. William Lindley MIT Lincoln Laboratory F124 A, P. O. Box 73 Lexington, MA 02173	1
Dr. R. M. Malbon/M.S. 1C Avantek, Inc. 3175 Bowers Avenue Santa Clara, CA 94304	1	Commander U. S. Army Electronics Command V. Gelnovatch (DRSEL-TL-IC) Fort Monmouth, NJ 07703	1
Mr. R. Bierig Raytheon Company 28 Seyon Street Waltham, MA 02154	1	RCA Microwave Technology Center Dr. F. Sterzer Princeton, NJ 08540	1
Dr. R. Bell, K-101 Varian Associates, Inc. 611 Hansen Way Palo Alto, CA 94304	1		

Hewlett-Packard Corporation Dr. Robert Archer 1501 Page Road Palo Alto, CA 94306	1	D. Claxton MS/1414 TRW Systems One Space Park Redondo Beach, CA 90278	1
Watkins-Johnson Company E. J. Crescenzi, Jr./ K. Niclas 3333 Hillview Avenue Stanford Industrial Park Palo Alto, CA 94304	1	Professor L. Eastman Phillips Hall Cornell University Ithaca, NY 14853	1
Commandant Marine Corps Scientific Advisor (Code AX) Washington, D. C. 20380	1	AIL TECH 612 N. Mary Avenue Sunnyvale, CA 94086 Attn: G. D. Vendelin	1
Communications Transistor Corp. Dr. W. Weisenberger 301 Industrial Way San Carlos, CA 94070	1	Professor Hauser and Littlejohn Department of Electrical Engr. North Carolina State University Raleigh, NC 27607	1
Microwave Associates Northwest Industrial Park Drs. F. A. Brand/J. Saloom Burlington, MA 01803	1	Professor J. Beyer Department of Electrical & Computer Eng. University of Wisconsin Madison, WI 53706	1
Commander, AFAL AFWAL/AADM Dr. Don Rees Wright-Patterson AFB, Ohio 45433	1	Professor Rosenbaum & Wolfe Semiconductor Research Laboratory Washington University St. Louis, MO 63130	1
Professor Walter Ku Phillips Hall Cornell University Ithaca, NY 14853	1	W. H. Perkins Electronics Lab 3-115/B4 General Electric Company P. O. Box 4840 Syracuse, NY 13221	1
Commander Harry Diamond Laboratories Mr. Forst W. A. Gerlach 2800 Powder Mill Road Adelphia, MD 20783	1		
Advisory Group on Electron Devices 201 Varick Street, 9th floor New York, NY 10014	1		

DATE
FILME
— 8